JOURNAL OF GEOPHYSICAL RESEARCH, VOL. 92, NO. A6, PAGES 5741–5762, JUNE 1, 1987

Io Plasma Torus Electrons: Voyager 1

E. C. SITTLER, JR.

Laboratory for Extraterrestrial Physics, NASA Goddard Space Flight Center, Greenbelt, Maryland

DARRELL F. STROBEL

Department of Earth and Planetary Sciences and Department of Physics and Astronomy Johns Hopkins University, Baltimore, Maryland

The analysis of in situ plasma electron observations in the Io plasma torus by the plasma science experiment during the Voyager 1 encounter with Jupiter is presented in terms of two components: a thermal (*c*) Maxwellian component and suprathermal (*H*) non-Maxwellian component of the electron distribution function. Average electron temperatures are $T_e < 1$ eV in the cold torus ($L < 5.5$), with $T_e \simeq 5$–6 eV in the hot torus ($5.5 < L < 7.6$); T_e rises abruptly to $T_e \simeq 30$ eV just outside the hot torus ($L > 7.6$) and then continues to rise to $T_e > 100$ eV at $r > 12\ R_J$. In the cold torus the density ratio of the suprathermal component n_H to that of the cold component n_c was $< 10^{-4}$; but in the hot torus, $n_H/n_C \sim 10^{-3}$ was observed, and outside the torus, n_H/n_c can exceed 10^{-1}. We present evidence that suprathermal electrons are locally produced in the hot torus. Throughout the hot torus the electron temperature T_e is a factor of 10 less than the thermal ion temperature. A large difference in the hot electron pressure P_H is observed between the inbound and the outbound data which is interpreted as a latitudinal gradient with P_H being a maximum at the magnetic equator. If one imposes the theoretical and observational constraint that $(T_\perp/T_\parallel)_{EQ} \leq 2$ for the hot electrons, then one requires the presence of a parallel electric field $E_\parallel > 2.5\ \mu V$/m which exceeds the ambipolar electric field $E_\parallel < 1\ \mu$V/m produced by the centrifugally confined ions. However, if unacceptable charge imbalances in the thermal plasma are not to occur from this larger $E_\parallel$, then sufficient wave turbulence in the plasma must be present to adequately scatter the thermal electrons. We infer the presence of a neutral corona around Io from the observed decrease and symmetry with respect to Io of T_c. The energy input to the torus by charge exchange and ionization in this neutral corona followed by pickup is $\sim 2 \times 10^{11}$ W, substantially less than the EUV luminosity. In the hot torus, suprathermal electrons contribute significantly to the ionization of the more highly ionized ions (O^+, O^{2+}, S^{2+}, and S^{3+}).

1. INTRODUCTION

Since *Carlson et al.* [1975] showed that electron impact ionization was the dominant ionization mechanism of Io's neutral sodium cloud, it has become increasingly evident that electrons play a major role in the physics of the plasma environment around Io. The importance of electrons was underscored by the discovery of the hot Io plasma torus by the Voyager 1 ultraviolet spectrometer experiment (UVS) [*Broadfoot et al.*, 1979]; almost all the UV emission observed from the torus was attributed to collisional excitation of ions by electrons. Through impact ionization, electrons make a major contribution to the ionization of neutrals and ions within the torus and thus control the degree of ionization within the torus. The pickup energy acquired by newly born ions is transferred to the electrons and provides the principal mechanism for energizing the torus [*Broadfoot et al.*, 1979; *Brown*, 1981; *Smith and Strobel*, 1985]. The importance of in situ electron observations for ground-based and spacecraft line-of-sight observations of the torus cannot be overstated. Line-of-sight observations are integral measurements over the spatial gradients of the system; models of the torus must be constructed in order to extract local information about the plasma within the torus. The more accurate the model, the more accurately one can reconstruct local plasma parameters from these line-of-sight observations. But there is no assurance of a unique determination of local quantities. In situ measurements of ions and electrons within the torus provide "ground" truth for these models of the torus and will ultimately improve interpretation of these line-of-sight observations.

In this paper we present results from analysis of in situ plasma electron observations made by the plasma science experiment (PLS) on Voyager 1 during its passage through the Io torus. In an initial analysis by *Scudder et al.* [1981] it was shown that the plasma electrons were composed of a cold and hot component and that significant radial and latitudinal gradients in the electron distribution function $f_e(r, v, t)$ were present.

In addition to the problems of spacecraft charging noted by Scudder et al., the previous analysis of the hot electron component was hindered by background signals produced by positive ions, which we refer to as "ion feedthrough." These effects have been corrected for in the present paper, and a detailed discussion of these feedthrough corrections can be found in the appendix. The paper is subdivided into eight sections. Section 2 presents trajectory information, and section 3 gives a brief description of the instrument and analysis pertinent to this paper. In section 4 a broad overview of the observations is first presented, followed by discussion and interpretation of these observations in section 5. Section 6 focuses on the Io flux tube passage and passage through a planetary scale neutral cloud (inferred from the electron observations) surrounding Io with dimension of $\lesssim 1\ R_J$. In section 7, electron impact ionization rates are computed from known energy dependent ionization cross sections and the observed electron distribution function along the spacecraft trajectory. Finally, a summary and concluding remarks are made in section 8.

Paper number 5A8362.
0148-0227/87/005A-8362$05.00

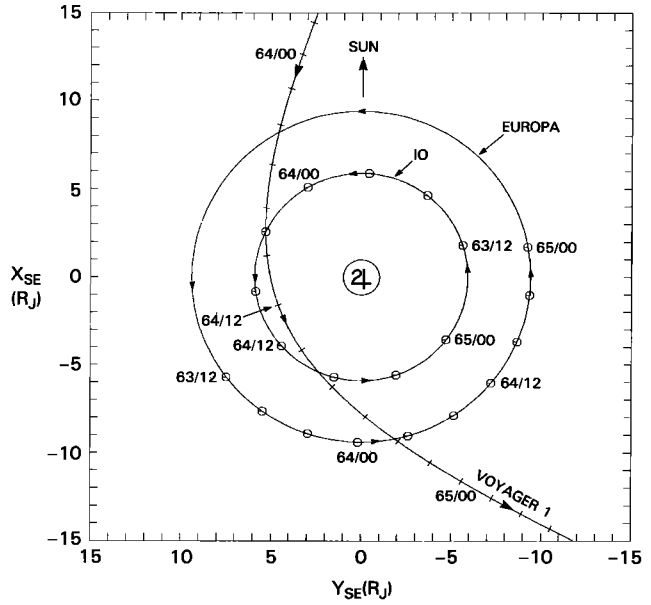

Fig. 1*a*. Equatorial view of Voyager 1 trajectory in a Jupiter-centered solar ecliptic coordinate system. Tic-marks along the trajectory are spaced 2 hours apart. Superimposed upon the trajectory are the nominal orbits of Io and Europa with their positions as a function of time indicated by circles, which are spaced 4 hours apart. The intersection of the Voyager 1 trajectory and Io's orbit after closest approach occurs near the Io flux tube passage.

2. VOYAGER 1 TRAJECTORY

In Figure 1 the Voyager 1 trajectory in a Jupiter-centered coordinate system for all of March 5, 1979 (day 64), is shown. Figure 1*a* gives an equatorial view of the trajectory in a solar ecliptic coordinate system with the motion of Io and Europa indicated, while in Figure 1*b* a meridional view is given with the vertical distance z measured in relation to the centrifugal equator. For orientational purposes we have superimposed the ion charge density contours from *Bagenal et al.* [1985] upon the trajectory plot in Figure 1*b*. Figure 2 gives a time plot of the dipole L shell parameter, magnetic latitude λ_M, centrifugal latitude λ_c, and system III longitude ϕ_{III}. To make this plot, we have used the dipole part of the O_4 model with tilt and offset by *Acuña et al.* [1983].

At the beginning of day 64 during the inbound pass the spacecraft was near the magnetic and centrifugal equators; it then proceeded to higher latitudes where it crossed the Europa L shell between 0401 and 0436. During the inbound

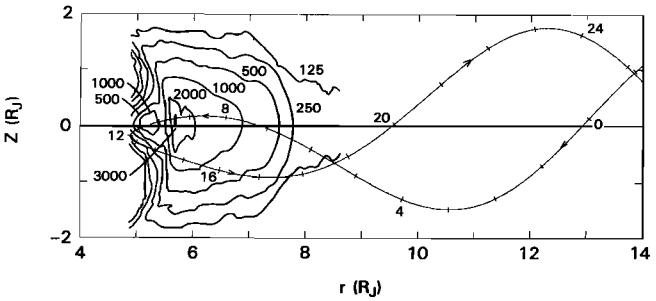

Fig. 1*b*. Meridional view of Voyager 1 trajectory plotted versus radial distance from Jupiter center and vertical distance Z relative to the centrifugal equator. For orientational purposes we have superimposed the total ion charge density contours for the Io plasma torus from *Bagenal et al.* [1985].

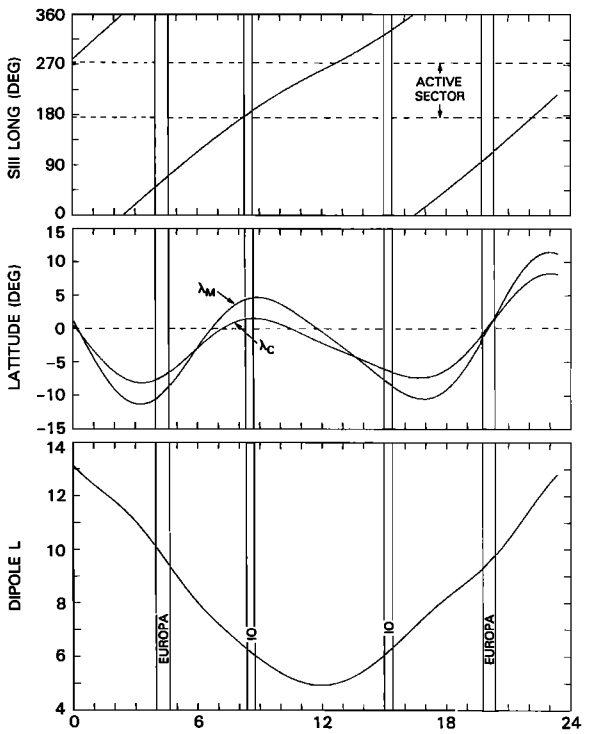

Fig. 2. Plot of dipole L, magnetic latitude λ_M, centrifugal latitude λ_c, and system III longitude ϕ_{III} versus time for all of March 5, 1979. To compute L, λ_M, and λ_c, we have used the O_4 dipole part of the model with tilt and offset by *Acuña et al.* [1983]. The vertical bars indicate the L shell crossing times for Io and Europa for which we have used the magnetic field model with ring current from *Connerney et al.* [1981]. The active sector as given by *Dessler and Vasyliunas* [1979] is indicated in the top panel for ϕ_{III}.

passage of the Io torus from 0630 to 1100 it was near the centrifugal equator, while during the outbound passage through the Io torus from 1400 to 1700 it was at high southerly latitudes. The spacecraft then crossed the Europa L shell between 1946 and 2022 near the magnetic and centrifugal equators. At the end of day 64 it was at $\lambda_M \approx 10°$ with a high northerly latitude trajectory.

3. INSTRUMENTATION AND ANALYSIS

Detailed information about the PLS instrument is given in the publication by *Bridge et al.* [1977], while information about the electron analysis is available in the publications by *Scudder et al.* [1981], *Sittler et al.* [1983], and *Sittler* [1983]. In this section we will confine our discussion to those features of the instrument and analysis which are directly relevant to this paper.

The PLS instrument is composed of four potential modulated Faraday cups which make positive ion and electron measurements within the energy range from 10 V to 5950 V. Electron measurements are made by the side sensor or D cup only, which uses two energy scan modes, E1 (10–140 eV) and E2 (140–5950 eV). Both energy modes are composed of 16 contiguously spaced energy channels which can be shown to be differential in relation to the electron distribution function f_e. They are individually sampled in 3.84 s but separated in time by 45 s. The side sensor has a fairly broad angular response with conical half angle of 30° (full width at half maximum) about the sensor look direction. Since electron measurements are made by only one sensor and the spacecraft is three-

axis stabilized, angular information about f_e is not available except for those infrequent periods when roll maneuvers are performed.

Although the D cup was favorably aligned to observed the nearly corotating cold ions during the inbound pass of the Io plasma torus, this orientation also allowed large ion feedthrough corrections to be present in the hot electron measurements within the high-density portions of the torus during the inbound pass (see appendix). These correction currents can exceed 80% of the measured signal. Within those regions where these corrections exceed 75% of the measured signal, we consider the analysis of the hot electrons preliminary, with accuracies in the suprathermal electron density n_H and pressure P_H to be no better than a factor of 2. During the outbound pass, except for a brief maneuver near the Europa L shell crossing, the D cup field of view was not favorably aligned to see the high-density, nearly corotating cold ions. Therefore during the outbound pass the ion feedthrough corrections were not important, and the hot electron measurements acquired during this period are considered reliable with accuracies of $\lesssim 30\%$ for n_H and P_H.

Because of the instrument's wide field of view it integrates over any angular variation in the electron distribution function such as a pressure anisotropy. Therefore if the pressure anisotropies were not large ($T_\perp/T_\parallel \sim 1$), the measurements provide a fairly accurate measure of the mean thermal energy of the electrons. In the case of the cold electrons within the Io torus, isotropization time scales τ_{isop} ($\sim$ minutes) are so much less than the residence time scales τ_{res} ($\sim$1–2 months) [*Smith and Strobel*, 1985; *Summers and Siscoe*, 1985] that one expects the cold electrons to be Maxwellian and isotropic. Model fits for the cold electron temperature component T_c should have an accuracy better than 10% with computed 1σ errors generally less than a few percent. Because the Coulomb mean free path, $\lambda_{Coul} > 10\ R_J$ for $E > 10$ eV electrons, is large in comparison to the characteristic scale lengths within the torus ($L \sim 1\ R_J$), the observed thermal electrons behave as a collisionless gas, and pressure anisotropies $T_\perp/T_\parallel \neq 1$ can occur.

The instrument integrates over the transverse component of f_e and provides a measurement of the reduced distribution function F_e which includes modifications produced by its angular response. By using an inversion technique discussed by *Sittler* [1983], the measured function F_e is decomposed into a Maxwellian for the cold electron component F_c and up to three Maxwellian components for the hot electron component F_H. Then f_e is computed from the multi-Maxwellian fit to F_e. Once f_e is known, moment estimations of n_e and T_e as discussed by *Scudder et al.* [1981] are straightforward. Details of the fitting procedure are discussed by *Sittler* [1983].

As noted by *Scudder et al.* [1981], within the Io plasma torus where electron densities n_e exceeded 1000 cm^{-3}, the spacecraft charged to a negative potential. When the spacecraft becomes negatively charged, the return current relation used by *Scudder et al.* [1981] is no longer valid, and some other other means must be used to estimate n_e and the spacecraft potential Φ_{SC}. This problem has been solved by using the charge neutrality condition described by Scudder et al. and independent estimates of the electron density from the PLS ion measurements [*McNutt et al.*, 1981; *Bagenal and Sullivan*, 1981; *Bagenal et al.*, 1985; R. L. McNutt, private communication, 1983] and from the planetary radio astronomy experiment (PRA) [*Birmingham et al.*, 1981].

4. Survey of Electron Observations

Electron Density and Temperature

Figure 3 is a time plot of the moment estimated total electron density n_e, total electron temperature T_e, and spacecraft potential Φ_{SC} for all of March 5, 1979. For reference we have added on top the system III longitude, centrifugal latitude, magnetic (dipole) latitude, and dipole L shell. Before 0415 and after 1940 the electron density was computed from the PLS electron data alone. During these periods when the electron density was < 100 cm^{-3}, the spacecraft was known to be positively charged, and the return current relation described by *Scudder et al.* [1981] was used to determine the spacecraft potential. From 0415 to 1940 the spacecraft was negatively charged (except for brief periods from 0458 to 0550 and from 0614 to 0635), and the independent estimates of n_e noted above along with the charge neutrality condition described by Scudder et al. were used as follows. From 0415 to 1400 the PLS total ion charge densities from *McNutt et al.* [1981] were used because the PLS main sensors were sufficiently aligned to observe the high Mach number, nearly corotating cold ions. From 1400 to 1830 the PRA electron densities from *Birmingham et al.* [1981] were adopted, since the PLS sensors were not favorably aligned to see the cold ions. As discussed in the appendix, the spacecraft was probably negatively charged in the brief interval from 1830 to 1940, and "predicted" total ion charge densities n_{ion} were used to fill in this gap. The charge densities n_{ion} were computed from a scale height model using the inbound PLS ion analysis of *Bagenal and Sullivan* [1981] and *Bagenal et al.* [1985] and the preliminary ion analysis by R. L. McNutt (private communication, 1983) and then mapped to those times with identical L shells during the outbound pass using the magnetic dipole field model of *Acuña et al.* [1983].

The inbound and outbound density profiles display a large-scale increase in n_e with decreasing L until the inner edge of the hot torus at $L = 5.5$ is reached. Inside $L = 5.5$, i.e., the cold torus, there is a general decrease in n_e except for the brief maximum when the spacecraft crossed the centrifugal equator at 1030 ($L = 5.2$). The inbound and outbound n_e were ~ 10 cm^{-3} at 13 R_J, with abrupt increases during the inbound pass at 0500 ($L = 9.0$) where n_e rose to 100 cm^{-3} and at 0630 ($L = 7.6$) where n_e abruptly increased to more than 1000 cm^{-3}. During the outbound pass, when the spacecraft is moving toward lower centrifugal latitudes, a similar but more smoothly varying profile is observed. Inflection points can be seen at 1715 ($L = 7.7$) and 1930 ($L = 9.1$) which nearly coincide in L with the corresponding boundaries noted above for the inbound pass; therefore azimuthal symmetry (see appendix) in n_e is roughly supported by the observations. The spatial regime from $L = 7.6$ to $L = 5.5$ where n_e exceeds 1000 cm^{-3} is referred to as the hot plasma torus.

The T_e profile displays a large-scale positive radial gradient for inbound and outbound passes. At 13 R_J, T_e is of the order of 100 eV, decreases to <6 eV for $L < 6.8$, and finally drops to less than 2 eV within the cold torus ($L < 5.4$). Between 1000 and 1350 ($L < 5.4$), no detectable electron fluxes above 10 eV were observed, and we attribute this lack of detection to $T_e <$ 2 eV in the cold plasma torus. (This upper limit for T_e is determined by the minimum electron flux that can be measured by the PLS instrument in the lowest E1 energy channel and the known ion charge densities from the PLS ion analy-

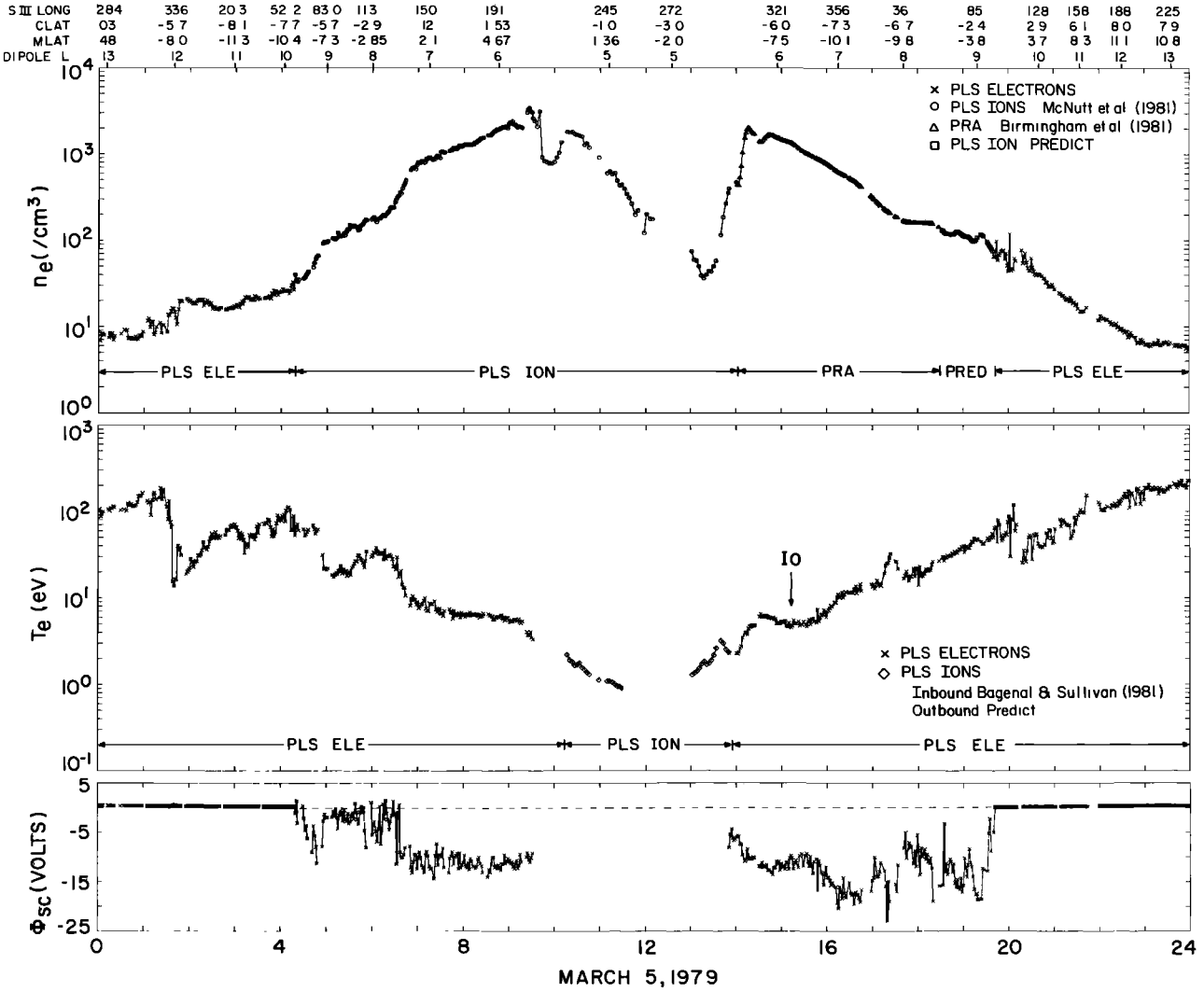

Fig. 3. Plot of the total moment electron density n_e, total moment electron temperature T_e, and spacecraft potential Φ_{SC} versus time for all of March 5, 1979 (day 64). The symbols used for the different data sets are denoted in the figure. We have also indicated at the bottom of the n_e and T_e panels the source of the data (PLS ELE is PLS electron data, PLS ION is PLS ion data from *Bagenal et al.* [1985] and R. L. McNutt (private communication, 1983), PRA is n_e inferred from PRA data from *Birmingham et al.* [1981], and PRED is scale height model predicted from inbound ion data (see appendix)). See text for details. On top we have indicated the system III longitude, centrifugal latitude, magnetic latitude, and dipole L.

sis.) Because of the short thermal equilibration time scales τ_{eq} (approximately hours) between ions and electrons and the long radial inward diffusion time scales τ_D (a few hundred days or more) (see section 5) within the cold torus we have set $T_e = T_i$ for the period from 1000 to 1350 (see discussion in the work by *Bagenal* [1985]). However, if a local heat source is present as *Moreno and Barbosa* [1986] favor, then $T_i > T_e$ as a result of radiative losses, and T_e would vary in parallel with T_i but never converge to it. Thus T_e actually may be less than the T_i values adopted here, and the reader should exercise caution. From 1300 to 1351, predicted values of the ion temperature were obtained by taking ion temperatures from the inbound pass [*Bagenal et al.*, 1985] and mapping them onto identical L shells during the outbound pass using the dipole part of the *Acuña et al.* [1983] model. On the basis of the ion data, electron temperatures of <1 eV are expected within the cold plasma torus.

Temperature of Cold Electron Component

Electron temperatures of the cold component, T_c, on March 5, 1979, are presented in Figure 4. To facilitate comparison between inbound and outbound values of T_c, we have mapped the inbound values of T_c to the outbound region using the L shell map described above. We also show in Figure 4 mean ion temperatures T_{ion} computed from the preliminary inbound analysis by R. L. McNutt (private communication, 1983) for times before 0500 and the inbound analysis by *Bagenal and Sullivan* [1981] and *Bagenal et al.* [1985] from 0500 to 1132. Between 1230 and 2400, predicted values of T_{ion} based on the inbound analysis are used with the same L shell map as above. It is clear from Figure 4 that the T_{ion} exceed T_c by more than an order of magnitude within the hot plasma torus. As discussed before, T_{ion} approaches T_c at the boundary separating the cold and hot torus.

Many of the features displayed in Figure 3 for T_e are also seen for T_c. This is not unexpected, since as shown below, the cold electron component dominates the total electron density and pressure within the PLS energy range. During the inbound crossing of the hot torus outer boundary at 0630 there is an abrupt decrease in T_c from 20 eV at $L = 7.7$ to less than 6 eV at $L = 6.8$. T_c gradually decreases to 5 eV at $L = 6$. A similar abrupt rise in T_c is seen during the outbound crossing of the outer boundary of the hot plasma torus.

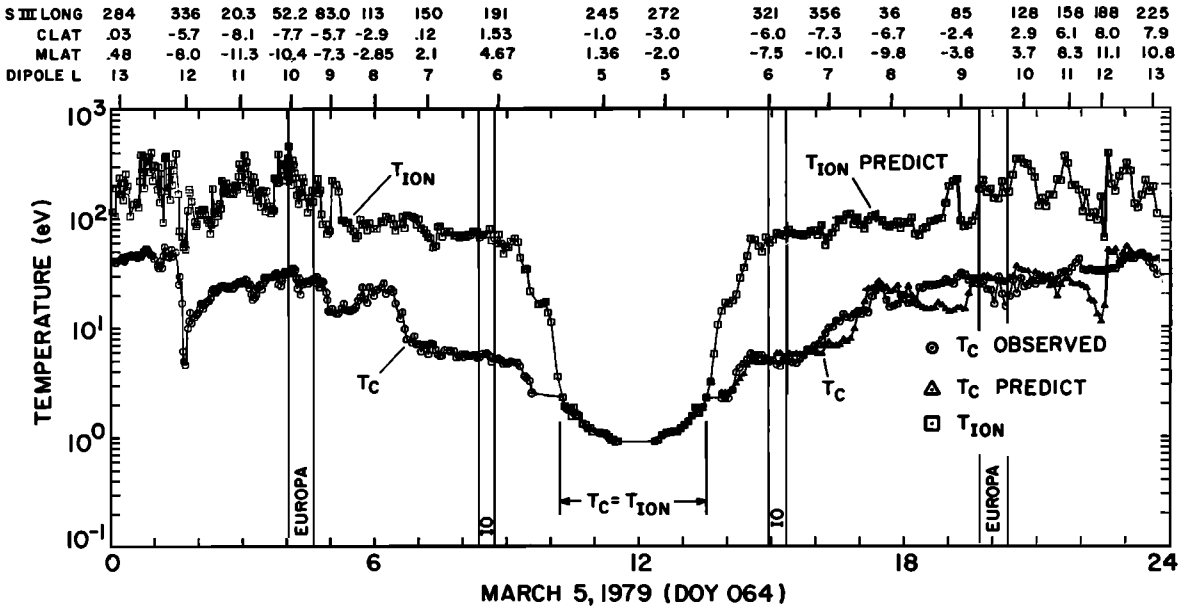

Fig. 4. Time plot of the cold electron temperature T_c (circles), predicted estimate of T_c (triangles) (see text for details), and mean ion temperature T_{ion} (squares) computed from the inbound analysis by *Bagenal and Sullivan* [1981], *Bagenal et al.* [1985], and the preliminary analysis by R. L. McNutt. The outbound estimates are computed from the L shell mapping technique discussed in text. Data coverage is for all of March 5, 1979 (day 64). As in Figure 2, the L shell crossing times for Io and Europa are indicated. On top we have indicated the system III longitude, centrifugal latitude, magnetic latitude, and dipole L.

Hot Electron Observations

In Figure 5 we have plotted the hot electron density n_H and hot electron pressure P_H as a function of time along with ratios in the bottom two panels of n_c/n_H and T_c/T_H. The hot electron parameters n_H, T_H, and P_H were computed by extrapolating the Maxwellian fit to the low-energy portion of the hot component, just above the break in the spectrum separating the cold and hot electrons, to zero energy. This tends to eliminate any variations in the cold electron component (movement of break in spectrum) from affecting the estimations of n_H, T_H, and $P_H = n_H k T_H$ (k is the Boltzmann constant in electron volts). As discussed in the appendix, the region marked A in the top panel has ion feedthrough corrections greater than 75% of the measured signal, and the parameter estimations in this region are preliminary.

Overall, the time profiles for n_H and P_H are very similar, although P_H displays less variability than n_H. Near the beginning of day 64 when $\lambda_M \sim 0°$, the density $n_H \approx 0.5$ cm^{-3}. From 0000 to 0140 the pressure P_H shows little change as the spacecraft moves to higher latitudes and smaller r, while n_H shows an increase with time. The parameters n_H and P_H undergo a sudden decrease from 0140 to 0230, when there is a sudden increase in cold plasma (plasma sheet crossing) which is colder than plasma in surrounding regions (see Figure 4 and *McNutt et al.* [1981]), and gradually increase until 0400, when the Europa L shell is approached. This general rise in n_H and P_H from 0000 to 0400 occurs when the spacecraft is moving to higher λ_M and must therefore reflect a radial and/or azimuthal variation in these parameters (since the magnetic mirror force will tend to enhance suprathermal fluxes at the magnetic equator). There is a localized minimum in n_H and P_H between 0455 and 0540 with little variation for the remainder of the inbound pass until 0930. Since little variation in λ_M occurs during this passage through the hot torus, the radial gradient in n_H and P_H must be small within the hot torus. After 0930 the analysis becomes very difficult because of interference and greater difficulty in modeling the ion feedthrough currents (see appendix).

The outbound data display a steep positive radial gradient in n_H and P_H between 1400 and 1430 spacecraft event time (SCET), which corresponds to the inner edge of the hot torus ($L = 5.5$). When mapped onto the inbound data, the abrupt rise in n_H at 1400 ($L = 5.5$), the plateau from 1410 to 1425, and the sudden rise after 1425 ($L = 5.75$) nearly coincide in dipole L with similar variations in T_{ion} reported by *Bagenal and Sullivan* [1981] for the inbound data. Therefore if the ion and electron features have a similar origin, this feature must be fairly broad in azimuth and probably extends all around the planet.

From 1430 to 2000 we see an overall decrease in n_H and P_H as the spacecraft moves to higher latitudes, with P_H displaying a broad minimum between 1530 and 1710 when $|\lambda_M| > 10°$. This variation is probably due primarily to a latitudinal effect, e.g., the magnetic mirror force, because the corresponding period during the inbound pass lacks a radial variation in P_H. The sudden increase in n_H and P_H at 1710 ($L = 7.6$) nearly coincides with the outer boundary of the hot torus. Near the outer edge of the Europa L shell crossing we note a sudden decrease in n_H and P_H after which very little change in these parameters is observed with increasing radial distance and magnetic latitude. This sudden drop in n_H and P_H, just outside the Europa L shell, for both inbound and outbound crossings, implies there is a source of hot electrons inside Europa's L shell, with satellite sweeping causing the drop in flux outside its L shell.

Outside the hot torus ($L > 7.6$) the ratio for n_c/n_H varies between 10 and 100, while the ratio T_c/T_H varies between 0.5 and 0.1. Within the hot torus, where the density of the cold component n_c exceeds 1000 cm^{-3} and the temperature of the cold component is considerably lower ($T_c \sim 5$ eV versus 20–30 eV outside the torus), the ratio n_c/n_H is approximately 10^3, and T_c/T_H is less than 10^{-2}. In the cold torus the ratio n_c/n_H can exceed 10^4. These large ratios for n_c/n_H are in rough

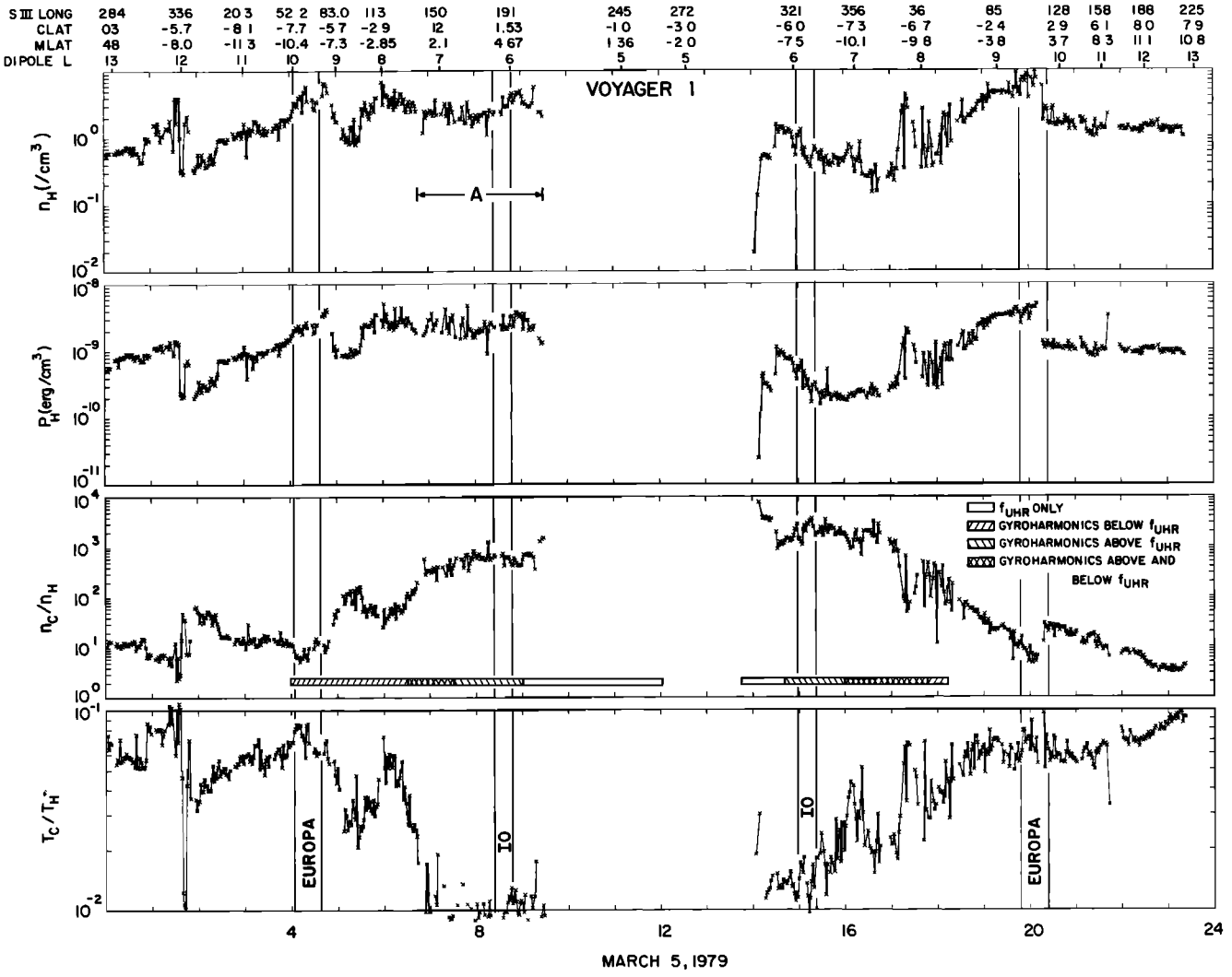

Fig. 5. Time plot of the moment hot electron density n_H, moment hot electron pressure P_H, ratio of n_c/n_H, and ratio of T_c/T_H for all of March 5, 1979 (day 64). On top of the figure we have indicated the system III longitude, centrifugal latitude, magnetic latitude, and dipole L. As in Figures 2 and 4, the dipole L shell crossing times for Io and Europa are shown. The letter A denotes the region where the hot electron analysis is preliminary because of ion feedthrough corrections. The horizontal bars in the second panel up indicate those regions of different plasma wave character as defined by *Birmingham et al.* [1981] using PRA observations.

agreement with the ground-based optical observations reported by *Brown et al.* [1983*b*], who set an upper limit of 2×10^{-4} for the ratio n_H/n_c in the post–Voyager 2 epoch on the basis of nondetection of O^{2+}.

5. Discussion and Interpretation

Cold Electron Component

Most of the EUV emission observed by the UVS experiment on Voyager is confined to the hot torus with maximum intensity at about 5.7 R_J [*Broadfoot et al.*, 1979; *Sandel et al.*, 1979]. From UVS observations at this radial distance, *Shemansky and Smith* [1981] inferred a cold electron temperature $T_c = 6.9$ eV. During the inbound pass when the spacecraft was near the centrifugal equator, in the highest-density regions of the hot torus ($n_e > 1800$ cm^{-3}, radial range 6.1–5.9 R_J, and times 0837–0858) and not in the vicinity of Io, the comparable in situ measurement was $T_c = 5.06$ eV $\pm$ 0.2 eV (see Figure 4). The apparent discrepancy between the PLS and UVS estimates of $\sim$1.8 eV. Recent analyses by *Smith and Strobel* [1985] and *Shemansky* [1987] are in agreement with the lower in situ values of T_c.

In Figure 4 we searched for local time, system III longitude, and latitudinal variations in T_c by superimposing predicted values of T_c, based on inbound estimates, upon the outbound estimates of T_c (see section 4). No systematic variation in T_c with local time, λ, or ϕ_{III} can be seen. If one considers the large-scale minimum in T_c centered on the Io flux tube crossing as a local effect, then within the hot torus there is a tendency for T_c to be greater during the outbound pass than in the inbound pass. Between 1600 and 1700 the difference in T_c inbound and outbound can be more than 50%. It can be seen from Figure 2 that the spacecraft is at higher magnetic and centrifugal latitudes during the outbound pass (1400–1700) than during the inbound pass (0635–0933). Also, the discrepancy between T_c (outbound) and T_c (inbound), within the hot

torus, becomes greater as the difference in latitude increases. Qualitatively, this tendency for higher temperatures at higher latitudes can be understood in terms of particle motion in a confining magnetic field with no collisions. For example, as the particle moves to higher λ_M where the magnetic field strength is greater, its parallel energy is converted to perpendicular energy, since the particle's total energy ($1/2mv^2 = 1/2mv_{\|}^2 + 1/2mv_{\perp}^2 = \text{const}$) and first adiabatic invariant ($v_{\perp}^2/B = \text{const}$) are conserved. Since the electron sensor is looking nearly perpendicular to the magnetic field for both inbound and outbound passes (see appendix), the instrument should observe an increase in T_c with increasing λ_M (i.e., instrument measures $T_{c\perp}$). Coulomb collisions will tend to reduce the presence of an anisotropy, but as discussed in section 2 the Coulomb mean free path for the cold electrons is large in comparison to the plasma scale height $H \sim 1\ R_J$, and a latitudinal gradient in $T_{\perp}/T_{\|}$ could persist.

We note that there was an observed decrease in T_c from 5.1 to 4.6 eV when the angle θ_{BN} between the D cup normal and magnetic field B changed from 90° to 135° during a roll maneuver at 1523 (cf. Figure A2). This change in T_c is consistent with $T_{\perp}/T_{\|} \sim 1.2$ for the cold electrons at $\lambda_M \sim -10°$ and supports the view that a pressure anisotropy in the thermal electrons is present.

We will next consider a possible relationship with ϕ_{III} and the active sector model by *Dessler and Vasyliunas* [1979]. Ground-based observations of the cold torus do show evidence of brightness variations at the system III period of 9.925 hours which appear to be caused by the active sector [*Trafton*, 1980; *Pilcher and Morgan*, 1980; *Trauger et al.*, 1980]. *Shemansky and Smith* [1981] found no evidence for a variation in the hot torus at the system III period, but recently, *Roesler et al.* [1984], *Sandel* [1983], and *Pilcher et al.* [1985] found brightness variations at a longer period of 10.2 hours (system IV [*Dessler*, 1985]). The brightness variations observed within the hot torus do not appear to have a direct relationship with the active sector. If one were to attribute the inbound-outbound difference in T_c to the magnetic anomaly model, then one would conclude that T_c was lower within the active sector than outside it, which is contrary to the prediction (prediction 1) by *Dessler and Vasyliunas* [1979]. The data may be consistent with the magnetic anomaly model in the context of a corotating convection electric field as proposed by *Hill et al.* [1981, 1983] for which there is plasma outflow in the active sector for $170° \leq \phi_{III} < 300°$. Recently, *Cheng et al.* [1984] reported a longitudinal asymmetry in Voyager 1 low-energy charged particle (LECP) phase space densities for ions and electrons within the Io plasma torus. This asymmetry has outbound fluxes greater than inbound fluxes at the same L shell and is similar to the T_c effect reported here. Although plasma flowing outward in the active sector should adiabatically cool, one might argue (A. J. Dessler, private communication, 1985) that on the basis of the observed increase in T_e with radius the mechanism of *Goertz* [1978] may apply in the active sector to produce a net heating of the outward flowing plasma.

We next consider the possibility of a local time effect which was detected in the EUV emissions of the hot torus [*Sandel and Broadfoot*, 1982; *Shemansky and Sandel*, 1982]. Theoretical explanations for this asymmetry have been proposed by *Barbosa and Kivelson* [1983] and *Ip and Goertz* [1983] in terms of a dawn-to-dusk convection electric field. From the analysis by Shemansky and Sandel they predicted a local time (LT) variation in T_c with a maximum value at 1900 LT and a minimum value at 0700 LT. The difference in T_c with local time tended to increase with radial distance within the hot torus. From Figure 1*a* it can be seen that the Voyager 1 spacecraft penetrated the hot torus at about 1600 LT during the inbound pass and 2240 LT during the outbound pass. Only a limited range of local times were sampled, and it is difficult to reach any definitive conclusions from out data set. In reference to Figure 5 of *Shemansky and Sandel* [1982] one would expect no significant difference between the inbound and outbound estimates of T_c, and one might conclude that the PLS electron observations are not in agreement with the predictions of *Shemansky and Sandel* [1982] if T_c has no λ or ϕ_{III} dependence. An alternative interpretation is that the predictions by *Dessler and Vasyliunas* [1979] and *Shemansky and Sandel* [1982] are correct and that the difference between the inbound and outbound data is a latitudinal effect.

Hot Electron Component

Scudder et al. [1981] demonstrated that the electron distributions have suprathermal tails. These hot electrons can provide a mechanism for rapid heating of the cold electrons through electron-electron collisions. Such a mechanism seems to be needed to account for the local time asymmetries (10% variations in T_c within 10 hours) observed by the Voyager UVS experiment [*Shemansky and Sandel*, 1982]. *Barbosa et al.* [1985] calculated an energy transfer time scale of ~0.9 hours via Coulomb collisions for a 100-eV electron interacting with a background component with $n_c \sim 2000\ \text{cm}^{-3}$ and $T_c \sim 5$ eV; in contrast, the typical energy transfer time scales between ions and electrons are >5 days. The hot electrons also provide the energy source for many of the plasma wave emissions observed by the Voyager plasma wave experiment (PWS) [*Scarf et al.*, 1979*a*] and the planetary radio astronomy experiment (PRA) [*Warwick et al.*, 1979].

Localized Source and Sink of Hot Electrons

Typical temperatures T_H for the suprathermal electrons within the hot torus are ~500 eV, so the Coulomb collisions will thermalize these electrons with the cold electrons in about 1 day ($\tau_{\text{therm}} \sim 10$ hours) while residence time scales are about 1–2 months [*Smith and Strobel*, 1985; *Summers and Siscoe*, 1985]. Therefore most hot electrons within the torus must be locally generated by some anomalous electron energization mechanism (see discussions by *Barbosa et al.* [1985]). The n_H and P_H profiles in Figure 5 show clear evidence for a source of hot electrons within the hot torus. The rapid drop in n_H and P_H at the boundary separating the cold and the hot torus ($L = 5.5$) defines the inner boundary of the hot electron source, while satellite sweeping by Europa at $L = 9.4$, inbound and outbound, provides a clearly defined outer boundary for the hot electrons. The source of these hot electrons must be confined inside Europa's L shell for this decrease to occur. Note that in the vicinity of Europa the ratio $\tau_{\text{therm}}/\tau_{\text{res}}$ could be ~1, as compared to ~0.01 in the Io torus, and therefore local generation of suprathermals in the vicinity of Europa need not occur.

The primary mechanism causing the depletion of hot electrons at the inner boundary of the hot torus is Coulomb collisions with cold electrons ($\tau_{\text{therm}} \sim 4$ days). Inelastic collisions with cold ions have longer time scales (~25 days). Since this depletion occurred over a distance of only 0.1 R_J, an inward

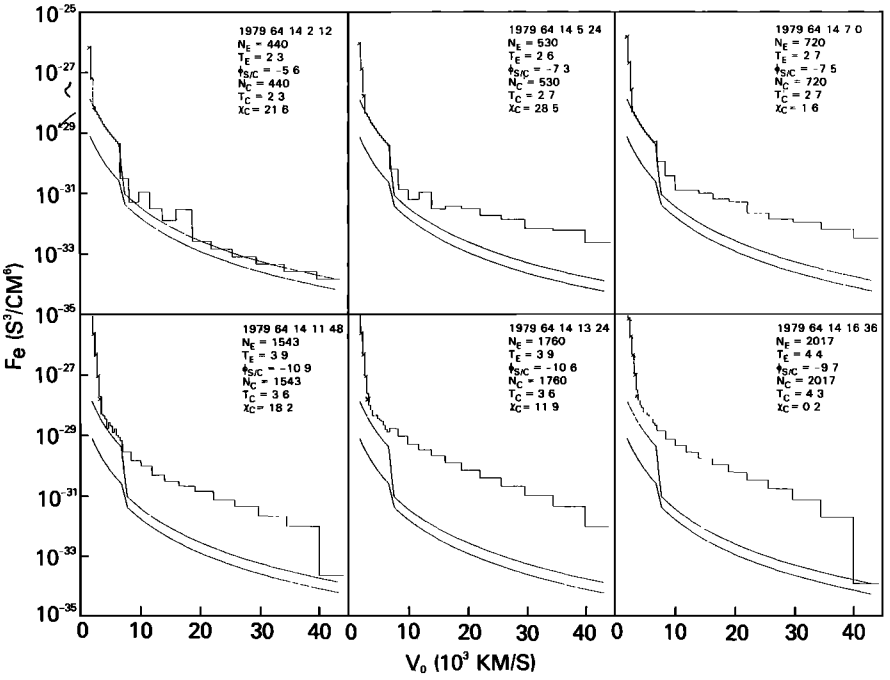

Fig. 6. Plot of the reduced electron distribution function F_e (see *Sittler* [1983] for definition) versus observed electron speed v_0 during the outbound traversal of the boundary separating the cold and the hot torus. Figure shows energy dependence of suprathermal electron depletion at this boundary. Spectrum time, moment estimated total electron density and temperature, spacecraft potential, cold electron density and temperature, and x^2 of cold component fit to spectrum are displayed in upper right-hand corner of each panel.

radial diffusion time scale τ_D of ~40 days over a radial distance of 1 R_J can be estimated. Theoretical arguments by *Siscoe et al.* [1981] imply a considerably longer diffusion time scale, and this fact suggests a weak source of hot electrons in the cold torus. At this inner boundary, auroral hiss was reported by *Gurnett et al.* [1979], which at earth is known to be associated with intense low-energy (10 eV to 1 keV) auroral electron precipitation [*Gurnett and Scarf*, 1983]. The electrostatic waves reported by *Birmingham et al.* [1981] could precipitate electrons below 100 eV (see, for example, *Barbosa and Kurth* [1980] and *Kurth et al.* [1983]). In Figure 6 we show the energy dependence of the hot electron depletions, from which it can be seen that this energy dependence is weak, with a tendency for the spectrum to become steeper as the spacecraft moves across this boundary. It is qualitatively consistent with energy loss by Coulomb collisions for which the collision frequency obeys a $1/E^{3/2}$ dependence. This is in sharp contrast to the hot electron depletions at Saturn, where the attenuations were greater at higher energies. The depletions at Saturn were believed to be caused by either electron precipitation induced by wave-particle interactions or collisions with micron-sized dust particles [*Sittler et al.*, 1983].

A number of mechanisms have been proposed for producing hot electrons within the torus. In the model by *Thorne* [1981], secondary electrons with energies of <1 keV are produced by energetic ions which precipitate into the auroral zone of Jupiter's upper atmosphere. The bulk of these secondary electrons have energies of ~20–40 eV and rapidly thermalize with the dominant cold electron component. This provides an energy source for the torus. Thorne estimated an energy input of $\sim 3 \times 10^{11}$ W for proton precipitation and $\sim 1.5 \times 10^{12}$ W for heavy ion precipitation if the energetic particle (30 keV to 1 MeV energies) precipitation is occurring at the strong diffusion limit. A suprathermal electron component with energies approaching 1 keV is produced by this process.

Barbosa et al. [1985] have proposed a different mechanism: production of hot electrons by growth of lower hybrid (LH) waves which are generated by newly picked-up ions within the hot torus. This mechanism produces a hot component with mean thermal energy $T_H \sim 1$ keV and $n_H/n_c \sim 10^{-3}$, which is in agreement with the observations shown in Figure 5. As shown in the work by Barbosa et al., the PWS data provide evidence for the presence of lower hybrid noise within the cold and hot torus with average wave amplitudes of 100 μV/m. Associated with this emission due to the ions is enhanced whistler mode emissions above 1 kHz caused by suprathermal electrons [*Scarf et al.*, 1979*a*, *b*] between the inner ($L = 5.5$) and outer ($L = 9.4$) boundaries of the hot electron region (see Figure 5). The hot ion fluxes observed by the PLS instrument display morphological features similar to those of the hot electrons. This supports the contention by *Barbosa et al.* [1985] that the hot ions are the source of the hot electrons. The hot ions display the same satellite sweeping signature at Europa's L shell, as well as reduced fluxes within the cold torus. The wave emissions below 1 kHz which have been identified as lower hybrid waves and whistler mode hiss by Barbosa et al. also have enhanced intensities inside Europa's L shell and outside the cold torus.

Outbound Roll Maneuver

An opportunity for obtaining pressure anisotropy information about the hot electrons occurred during the outbound roll maneuver just inside Europa's L shell crossing (1940–2000) when the spacecraft was near the magnetic equator. Figure 7 is a 2-hour plot centered on this roll maneuver of the moment estimated hot electron temperature T_H estimated

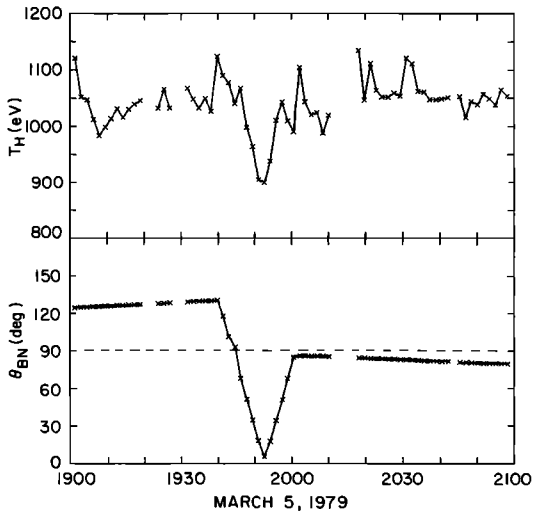

Fig. 7. Plot of the hot electron temperature T_H for electron energies of >650 eV and the angle θ_{BN} during the outbound roll maneuver near Europa's L shell; θ_{BN} is the angle between the magnetic field **B** and the D cup normal $\hat{n}_D$. Figure shows evidence for pressure anisotropy in the hot electrons with $T_\perp > T_\parallel$.

from a moment analysis for electron energies of >640 eV versus the angle between the D cup normal and the magnetic field θ_{BN}. At lower energies a similar dependence on θ_{BN} is observed, but not as clearly. From the observed dip in T_H centered on $\theta_{BN} = 0°$ one can estimate a pressure anisotropy $T_\perp/T_\parallel$ of at least ≈ 1.17 for the hot electrons. Because temperature variations before and after the roll maneuver are <5%, this dip in T_H is significant.

Latitudinal Dependence of P_H

We now consider the outbound variations in P_H for which the suprathermal fluxes maximized at the magnetic equator. Although temporal and azimuthal variations are evident in Figure 5, we assume all systematic variations displayed by the data are caused by radial and/or latitudinal dependences. The inbound profiles for P_H display very little radial dependence between the orbits of Io and Europa. During this period the spacecraft is confined closely to the magnetic and centrifugal equators (λ_M and $\lambda_c < 5°$ in magnitude) from 0600 to 0930. The decrease between 0440 and 0535 is considered temporal. The pressure from 0400 to 0440, when the spacecraft was about 9.5° below the magnetic equator, is about a factor of 2–3 higher than what would be inferred from the latitudinal variations of the outbound data with no assumed radial variation. The values for P_H between 0600 and 0930 when $|\lambda_M| < 5°$ are within a factor of 2 in magnitude to that observed near the outbound crossing of the magnetic equator at about 2000. With the above in mind we have taken the outbound data inside Europa's L shell and plotted 5-min averages of P_H versus λ_M in Figure 8. In addition to the expected λ_M dependence, the data show a hysteresis in λ_M associated with the crossing at $L \sim 7.7$ (1715 SCET) of the position of the EUV hot torus outer boundary. The lower curve is confined to $L < 7.7$. This boundary is not evident in the inbound data, which may be explainable in terms of an increase in vertical scale height of the hot electrons outside this boundary (i.e., $\lambda_M \sim 0°$ at $L \approx 7.7$ inbound and $\lambda_M \sim -10°$ at $L \approx 7.7$ outbound). This change in scale height could be caused by a change in pressure anisotropy such that $T_\perp/T_\parallel$ was less outside this boundary.

In an attempt to explain this latitudinal dependence on P_H, we have constructed a simple model for the parallel component of the momentum equation for hot electrons:

$$\frac{\partial P_{H_\parallel}}{\partial l} - (P_{H_\parallel} - P_{H_\perp})\frac{\partial}{\partial l}\log B + n_H e E_\parallel = 0 \qquad (1)$$

Here $P_{H_\parallel}$ and $P_{H_\perp}$ are the parallel and perpendicular components with respect to **B** of P_H, $E_\parallel = \hat{b} \cdot \mathbf{E}$ ($\hat{b} = \mathbf{B}/B$) is the field-aligned electric field, and $\partial/\partial l = \hat{b} \cdot \nabla$. To obtain closure, we have used the approach described by *Vasyliunas* [1983] and assumed the first and second adiabatic invariants, $P_{H_\perp}/n_H B$ and $P_{H_\parallel} B^2/{n_H}^3$, respectively, are constants. The first invariant, convervation of magnetic moment μ, is expected to be conserved; but conservation of the second invariant as given above may not hold. Solutions to (1) are obtained as a function of the pressure anisotropy $(T_\perp/T_\parallel)_{EQ}$ for the hot electrons at the magnetic equator, in a dipole field for B, and a specific form for $E_\parallel = E_\parallel(L, \lambda_M)$. In this model, $T_\perp/T_\parallel$ is an increasing function of $|\lambda_M|$.

Solutions to (1) with $E_\parallel = 0$ are given by curves 1 and 2 in Figure 8. The large λ_M dependence in P_H requires large pressure anisotropies $(T_\perp/T_\parallel)_{EQ} \gg 1$ because an excursion of less than 12° from the magnetic equator in a dipole field produces only a small change in B (i.e., $B(L, \lambda_M)/B(L, 0) < 1.21$ for $|\lambda_M| < 12°$). Deviations from a dipole field inside Europa's L shell due to the ring current modeled by *Connerney et al.* [1981] would provide an increase in the ratio of $B(L, \lambda_M)/B(L, 0)$ from 1.21 to 1.45 (J. E. P. Connerney, private communication, 1985), but this decreases $T_\perp/T_\parallel$ by no more than a factor of 2 and still leaves $T_\perp/T_\parallel \gg 1$.

These inferred anisotropies are considerably larger than those calculated from the outbound roll maneuver and are theoretically unexpected because of the isotropizing effects of Coulomb collisions, as well as effects of pitch angle scattering due to whistler mode waves when $T_\perp/T_\parallel > 1$ [*Kennel and Petschek*, 1966]. High inferred anisotropies are also in conflict with the models by *Thorne* [1981] and *Barbosa et al.* [1985].

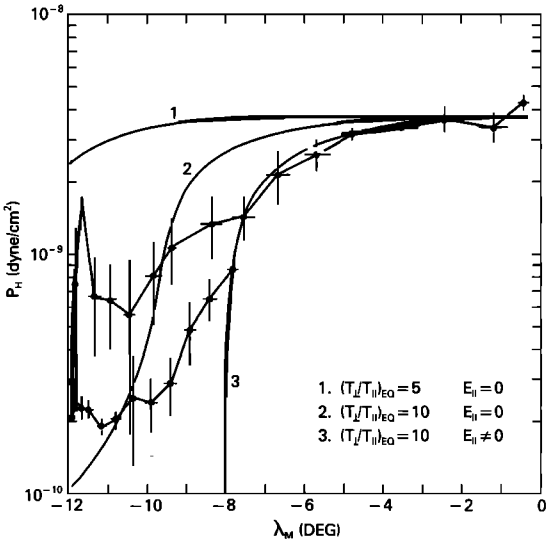

Fig. 8. Plot of the hot electron pressure P_H versus magnetic latitude λ_M for data acquired during the outbound passage of the hot torus. Theoretical curves allowing estimation of $(T_\perp/T_\parallel)_{EQ}$ for the hot electrons are superimposed (see text for details).

In Thorne's model the secondary electrons initially have equatorial pitch angles near 0° ($T_{\parallel}/T_{\perp} \gg 1$). Coulomb collisions are not expected to reverse the anisotropy so that $T_{\parallel}/T_{\perp} < 1$. Similarly, in the model by *Barbosa et al.* [1985] the lower hybrid waves will tend to accelerate the electrons along B [*Winske et al.*, 1985; H. K. Wong, private communication, 1985) so that $T_{\parallel}/T_{\perp} > 1$ is expected. However, the detection of chorus emissions at 0620 (outside the hot torus) by the Voyager 1 plasma wave instrument (PWS) was interpreted to be due to keV suprathermal electrons with pressure anisotropies $(T_{\perp}/T_{\parallel})$ of ~ 2 by *Coroniti et al.* [1980]. Therefore anisotropies $(T_{\perp}/T_{\parallel})_{EQ}$ of $\lesssim 2$ outside the hot torus cannot be excluded.

Finally, to try to reconcile our model predictions of $T_{\perp}/T_{\parallel} \gg 1$ with expectations and observations to the contrary, we have introduced a nonzero $E_{\parallel}$. Consider the possibility of an ambipolar electric field set up by the centrifugally confined thermal ion and electron populations with the following assumed polarization potential:

$$\Phi_{pol}(L, \lambda_M) = -\frac{1}{2}\left(\frac{T_e}{T_{ion} + Z_{ion}T_e}\right) A_{ion} \cdot \left(\frac{m_p}{e}\right)(\Omega_J R_J L_J)^2(1 - \cos^6 \lambda_M) \quad (2)$$

and

$$E_{\parallel}(L, \lambda_M) = -\frac{\partial \Phi_{pol}}{\partial l}$$

which applies for a single ion plasma in a dipole field with no tilt. A_{ion} is the ion mass in atomic mass units, Z_{ion} is the ion charge state, Ω_J is Jupiter's angular rotation frequency, R_J is a Jovian radius, m_p is a proton mass, and e is the unit electric charge. In Figure 8, curve 3 results when we set $A_{ion} = 32$, $Z_{ion} = 2$(composition S^{2+}), and $T_e = T_{ion}$ into (2) and introduce the resultant $E_{\parallel}$ into (1). In reality, T_e is less than $T_{ion}/3$, and the adopted $E_{\parallel}$ is an overestimate, but it shows the importance of an electric field. The solution provides a good match to the data for $|\lambda_M| < 8°$ with an equivalent anisotropy $(T_{\perp}/T_{\parallel})_{EQ} = 10$. More realistic models of $E_{\parallel}$ require a self-consistent scale height calculation similar to that of *Bagenal and Sullivan* [1981], but such models would not significantly increase the $E_{\parallel}$ magnitude. On the basis of the roll maneuver data, plasma wave observations of chorus emissions outside the hot torus, and theoretical expectations we require $T_{\perp}/T_{\parallel} \lesssim 2$, which implies larger $E_{\parallel} \gtrsim 2.5$ μV/m than predicted by (2). In estimating $E_{\parallel} \sim 2.5$ μV/m we took into account nondipole corrections to the magnetic field which decreased $E_{\parallel}$ by a factor of 2. Such corrections are not applicable within the hot torus. One way of generating such a large $E_{\parallel}$ is the thermoelectric $E_{\parallel}$ that *Hultqvist* [1970, 1971] (see also *Stern* [1981]) proposed for the earth's magnetosphere where field-aligned currents are produced by precipitating electrons, thus generating large $E_{\parallel}$.

The most obvious consequence of invoking such a large $E_{\parallel} \gtrsim 2.5$ μV/m is that the latitudinal thickness of the plasma torus would increase beyond the values deduced by *Bagenal et al.* [1985] and possibly that inferred from the inbound-outbound profile of n_e constructed from the PRA observations. However, a more serious consequence of this larger $E_{\parallel}$ is the charge imbalance between the ions and electrons which would occur. Inspection of the generalized Ohm's law equation

$$E_{\parallel} = -\frac{\nabla \cdot P_e}{n_e e} + \frac{m_e}{n_e e^2}\left(\frac{\delta j}{\delta t}\right)_{coll}$$

shows the presence of a resistivity term due to collisions. If this term is small, then $E_{\parallel}$ must equal the ambipolar electric field, and $(T_{\perp}/T_{\parallel})_{EQ} \gg 1$. If the resistivity term is large in comparison to the pressure gradient term, then the plasma can support such a large $E_{\parallel}$. Coulomb collisions can be shown to be inadequate, so that wave turbulence in the plasma must be present to provide adequate scattering of the thermal electrons. One possibility is the broadband wave emissions within the Io torus reported by *Scarf et al.* [1979*a*, *b*].

The lack of a significant latitudinal gradient in P_H from 0400 to 0600 during the inbound pass could be construed as providing evidence that a radial dependence was important during the outbound pass ($dP_H/dr > 0$), at least for $L > 8$. But temporal variations in P_H are also evident during this same time interval. So it is not clear whether the inbound data for $L > 8$ could be used as evidence against our interpretation for a latitudinal gradient in the outbound data. It is difficult to interpret the increase in P_H with r as a radial dependence for $L > 8$ outbound, since one expects a dilution effect from the increase in flux tube volume with r ($dP_H/dr < 0$ expected). Inside $L = 8$ our inference of a latitudinal gradient is more established, and the overall systematic variation of P_H with λ_M during the outbound pass strongly argues for a latitudinal dependence. (The possibility of an Io effect can be excluded from the difference in scale length between that expected for an Io effect and that observed.) It may also be true that there is a local time asymmetry in $E_{\parallel}$.

Half-Harmonic Electrostatic Waves

Birmingham et al. [1981] interpreted PRA observations of upper hybrid resonance (UHR) emissions and half-harmonic emissions above and below the UHR line position in terms of a bimodal distribution for the electrons within the Io torus, with the hot electron component having a loss cone anistropy. As shown in their paper and Figure 5, half-harmonic electrostatic waves are observed below the UHR emission line $f_{UHR} = (f_p^2 + f_g^2)^{1/2}$ in the outer torus, both above and below f_{UHR} at intermediate radial distances within the hot torus, above f_{UHR} within the inner portions of the hot torus, and only f_{UHR} emission within the cold torus. In their model calculations they determined that n_c/n_H must be $\gg 1$, which is supported by PLS observations displayed in Figure 5. They also determined that the ratio T_c/T_H should have a positive radial gradient in order to account for the movement of the half-harmonic emission from above f_{UHR} to below f_{UHR} with increasing radius. For half-harmonic emission above f_{UHR} they estimated $T_c/T_H < 0.02$, which is very close to that shown in Figure 5 for the inner regions of the hot torus. For $T_c/T_H \sim 0.04$, half-harmonic emission is confined below f_{UHR}, and this is approximately what is observed near the outer boundaries of the hot torus. Therefore, semiquantitatively, this effect is supported by the PLS observations. The lack of half-harmonic emission within the cold torus is probably due to the low suprathermal electron fluxes (T. J. Birmingham, private communication, 1983).

Chorus Emissions

Coroniti et al. [1984] reported the detection of chorus emissions by the Voyager 1 plasma wave experiment from 0457:35

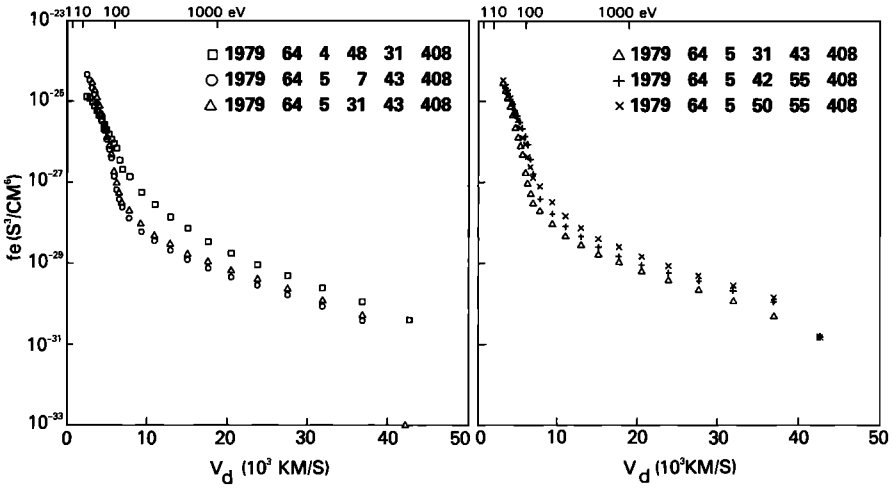

Fig. 9. Plot of the electron distribution function f_e for the time period *Coroniti et al.* [1984] reported no chorus emission. Figure shows a reduction in suprathermal fluxes centered on 500 eV during the time period chorus emission is not observed.

to 0630 SCET with a broadband chorus component between $0.25f/f_g$ and $0.45f/f_g$, a narrow-band chorus emission just above $0.5f/f_g$, and no emission between $0.45f/f_g$ and $0.5f/f_g$. We make no attempt here to comment about the theoretical explanations for this emission; we only wish to clarify some points made in that paper with regard to how they relate to the in situ electron observations. They noted that no chorus emission was evident in the plasma wave data from 0505 to 0542 SCET and suggested a reduction in the pitch angle anisotropy as the preferred explanation. Although the timing is not exact, one notes in Figure 5 a reduction in the suprathermal fluxes from 0457 to 0550 SCET with P_H dropping below 10^{-9} dyn/cm^2 at about 0500 and rising above 10^{-9} dyn/cm^2 at about 0540 SCET. Within this region the cold electrons also tend to be colder, with $T_c \approx 15$ eV inside, while outside this region, T_c is ≈ 20 eV. To see this more clearly, we show in Figure 9 a plot of the electron distribution function f_e before, during, and after this event. Of major importance is that the reduction in f_e maximizes at about 500 eV, a typical resonance energy discussed by Coroniti et al. for producing the chorus emissions. The lack of chorus emission from 0505 to 0542 is primarily caused by a reduction in the flux levels of the suprathermal electrons, but we agree with Coroniti et al. that the lack of chorus emission after 0630, when the spacecraft enters the Io plasma torus, is caused by an increased isotropization of the suprathermal electrons by Coulomb collisions due to the higher background densities within the torus, $n_e \sim 1000$ cm^{-3}, versus $n_e < 300$ cm^{-3} outside the torus.

6. IO'S NEUTRAL CORONA

The electron temperature data (Figure 3) in the vicinity of Io contain a signature which we tentatively attribute to a dense neutral corona or cloud around Io. In Figure 10 the cold electron temperature is plotted as a function of radial distance from the center of Io with the closest approach being the nominal passage through the predicted Io flux tube at 11.5 R_{Io} or $\simeq 0.3$ R_J. In this Io-centered coordinate system the cold electron temperature displays a symmetry with respect to Io. From a distance of 20 R_{Io} or 0.5 R_J where $T_e \simeq 5.5$ eV the electron temperature decreases to $\simeq 4.8$ eV at closest approach. In plasma penetrating a dense neutral cloud where considerable ionization is occurring, the electron density would be expected to build up. Because the newly picked-up electrons acquire only $\sim 10^{-2}$ eV of energy in the acceleration process and have little kinetic energy initially, the electron temperature would be expected to decrease.

From the geometry of Figure 1*a*, the time required for the corotating plasma to traverse a tangential distance of 0.4 R_J from the outer radius of 0.5 R_J to the point of closest approach to Io is 520 s. The observed electron temperature decreases by 0.7 eV with a time constant $\tau = (dT_e/dt\ T_e^{-1})^{-1} \sim 4 \times 10^3$ s, which is extremely short in comparison to the ion confinement or diffusion time. The question arises whether this observed decrease in T_e is generated locally in the vicinity of the spacecraft trajectory or produced nonlocally somewhere along the magnetic flux tube, perhaps in the vicinity of closest approach to Io. For $T_e = 5$ eV and $n_e = 2000$ cm^{-3}, we estimate a mean free path of ~ 1.4 R_J which is greater than the plasma scale height and indicative of a quasi-collisionless

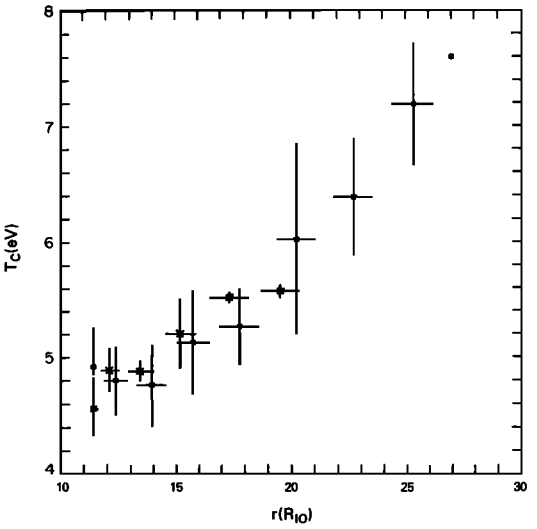

Fig. 10. Plot of the cold electron temperature T_c versus radial distance from Io for the time period centered about the Io flux tube passage. The crosses and squares are used for data acquired while the spacecraft approached and departed from Io, respectively.

plasma. A 5-eV electron traverses 1 R_J in 54 s, which is short in comparison to the traversal time of the corotating plasma. The time scale for electron self-collisions is ~ 74 s, while the time it takes newly picked-up electrons ($T \sim 10^{-2}$ eV) to thermally equilibrate with the ambient electron plasma ($T_e \sim 5$ eV) is ~ 45 s. On the basis of these time constants we conclude that the observed change in T_e is produced nonlocally, i.e., generated somewhere along the magnetic flux tube where the neutral density of Io's extended atmosphere (corona or exosphere) is highest.

Heat conduction by thermal electrons can rapidly transport thermal energy along magnetic flux tubes. In the collision limit the time constant for heat conduction driven by the 0.7-eV observed temperature change over a distance of 1 R_J is only ~ 3 s. Because the plasma probed by Voyager is quasi-collisionless, this time scale is obviously longer, of the order of the self-collision time scale (~ 74 s), which is still substantially smaller than the spacecraft traversal time.

To explore this hypothesis quantitatively, consider the continuity equation for electrons which is given as

$$\frac{dn_e}{dt} = \sum_{j=1}^{2} I_j N_j n_e - \frac{n_e}{\tau_D} \tag{3}$$

where the summation is over neutrals S and O with densities N_j, and I_j is their ionization rates by electron collisions. The electron energy equation may be written as

$$\frac{3}{2}\left(n_e \frac{dT_e}{dt} + T_e \frac{dn_e}{dt}\right) = \sum_{j=1}^{2} \varepsilon_j I_j n_e - \frac{\frac{3}{2} n_e T_e}{\tau_D} + q_{ie} - q_{\text{rad}} + \nabla_{\parallel} \cdot (\mathbf{q}_{\text{HC}}) \tag{4}$$

where q_{ie} is the Coulomb collisional energy transfer rate between the hotter ions and cold electrons, $\mathbf{q}_{\text{HC}}$ is the thermal electron heat flux, $\nabla_{\parallel}$ is the divergence along the B field, and q_{rad} is the ion EUV radiative loss rate due to electron collisional excitation; ε_j is the net energy added/subtracted in the ionization process. Because the ionization potentials (I.P.) of O and S are 13.6 and 10.4 eV, respectively, whereas $T_e \sim 5$–6 eV in the hot torus, most ionization of neutrals occurs by electrons at the threshold ionization energy. Newly picked-up electrons acquire only $\sim 10^{-2}$ eV; thus $\varepsilon_j \simeq -$I.P. of the neutral. Substitution of (3) into (4) yields

$$\tfrac{3}{2} n_e \frac{dT_e}{dt} = -\sum_{j=1}^{2} [(\text{I.P.})_j + \tfrac{3}{2} T_e] I_j N_j n_e + q_{ie} - q_{\text{rad}} + \nabla_{\parallel} \cdot (\mathbf{q}_{\text{HC}}) \tag{5}$$

When (5) is integrated over the entire torus volume, steady state conditions approximately apply, i.e., $dT_e/dt \simeq 0$, and $q_{ie} \simeq q_{\text{rad}}$.

Because q_{ie} and q_{rad} are functions of n_i, n_e, T_i, T_e, and not N_j, with time constants of 19 days and 0.8 day, respectively, the observed decrease in T_e near Io cannot be produced by q_{ie} and q_{rad} through changes in plasma parameters. This disparity in time constants is related to the fact that many photons must be radiated away to balance the energy transfer of 270 eV for O and 540 eV for S of pickup energy acquired by each newly created ion. Also, the time constant for q_{ie} is based solely on the collision frequency.

Thus the only terms in (5) which can account for the decrease in T_e are the first term on the right-hand side which is a function of the neutral density and the last term if there is a temperature gradient along **B**.

On the basis of the time constant arguments above we attribute the local observed dT_e/dt along the spacecraft trajectory to $\nabla_{\parallel} \cdot \mathbf{q}_{\text{HC}}$ and $\nabla_{\parallel} \cdot \mathbf{q}_{\text{HC}}$ to a nonlocal interaction of thermal electrons with newly created electrons on magnetic flux tubes at their closest approach to Io. Unfortunately, we do not know how the magnetic field lines are draped around Io, and the densities that we infer below cannot be assigned a precise radial position. Equation (5) can be written approximately as

$$\tfrac{3}{2} n_e \frac{dT_e}{dt}\bigg|_{\text{sc}} \simeq \nabla_{\parallel} \cdot \mathbf{q}_{\text{HC}}\bigg|_{\text{sc}} \simeq -\sum_{j=1}^{2} [(\text{I.P.})_j + \tfrac{3}{2} T_e] I_j N_j n_e\bigg|_{\text{Io corona}} \tag{6}$$

The Lagrangian or material derivative in (6) may be replaced by $v_p \, \partial T_e/\partial s$ where v_p is the plasma velocity and s is a measure of distance along the plasma trajectory. Equation (6) can be integrated to obtain

$$T_e(s) - T_e(\infty) = -\sum_{j=1}^{2} \frac{\frac{2}{3}(\text{I.P.})_j + T_e}{v_p} I_j \int_{R_{\text{exobase}}}^{\infty} N_j \, ds \tag{7}$$

where we have arbitrarily assumed that the magnetic field lines penetrate to the exobase of Io, which is approximately at $r = 1.5$–$2\ R_{\text{Io}}$ (M. E. Summers et al., The radial distribution of constituents in Io's corona and implications for atmospheric escape, submitted to *Journal of Geophysical Research*, 1987 (hereinafter Summers et al., 1987)), that the integral is performed along a radial path upstream from Io at closest approach, and that the plasma density remains approximately constant as it penetrates Io's corona. We do not attempt to model the radial variation of T_e, which requires further assumptions about the radial dependence of N_j. The radial variation of T_e does indicate that the corona extends to $\sim 0.4\ R_J$ from Io. From the definition of the exobase,

$$\int N_j \, dr \simeq 3 \times 10^{14} \text{ cm}^{-2}$$

Evaluation of the right-hand side of (7) with $T_e = 5.2$ eV for an atomic oxygen corona gives -1 eV and for a sulfur corona -6.5 eV, in comparison to the observed 0.7 eV. Based on the models of *Kumar* [1980], *Smith and Strobel* [1985], and Summers et al. (1987), the oxygen corona is appropriate for the Voyager 1 encounter, and our assumption that the plasma penetrates to the exobase is a realistic estimate. Actually, a rigorous derivation of (4)–(6) would include all electron-neutral inelastic collisions that cool the electron gas. This would lead to, at most, a factor of 2 reduction in the inferred neutral column density probed in the Io corona. The major experimental uncertainty is the location of the exobase. The PLS data cannot provide an answer, as closest approach to Io was only 11.5 R_{Io}. Currently, we are forced to rely on theoretical models.

The corresponding solution to the electron continuity equation can be written as

$$n_e = n_{e0} \exp\left(\sum_{j=1}^{2} \frac{I_j}{v_p} n_j\right) \tag{8}$$

Numerical results from (7) yield modest increases in n_e of 6.5–8% from ionization of neutrals by electron impact in the corona. A comparison of the inbound and outbound electron

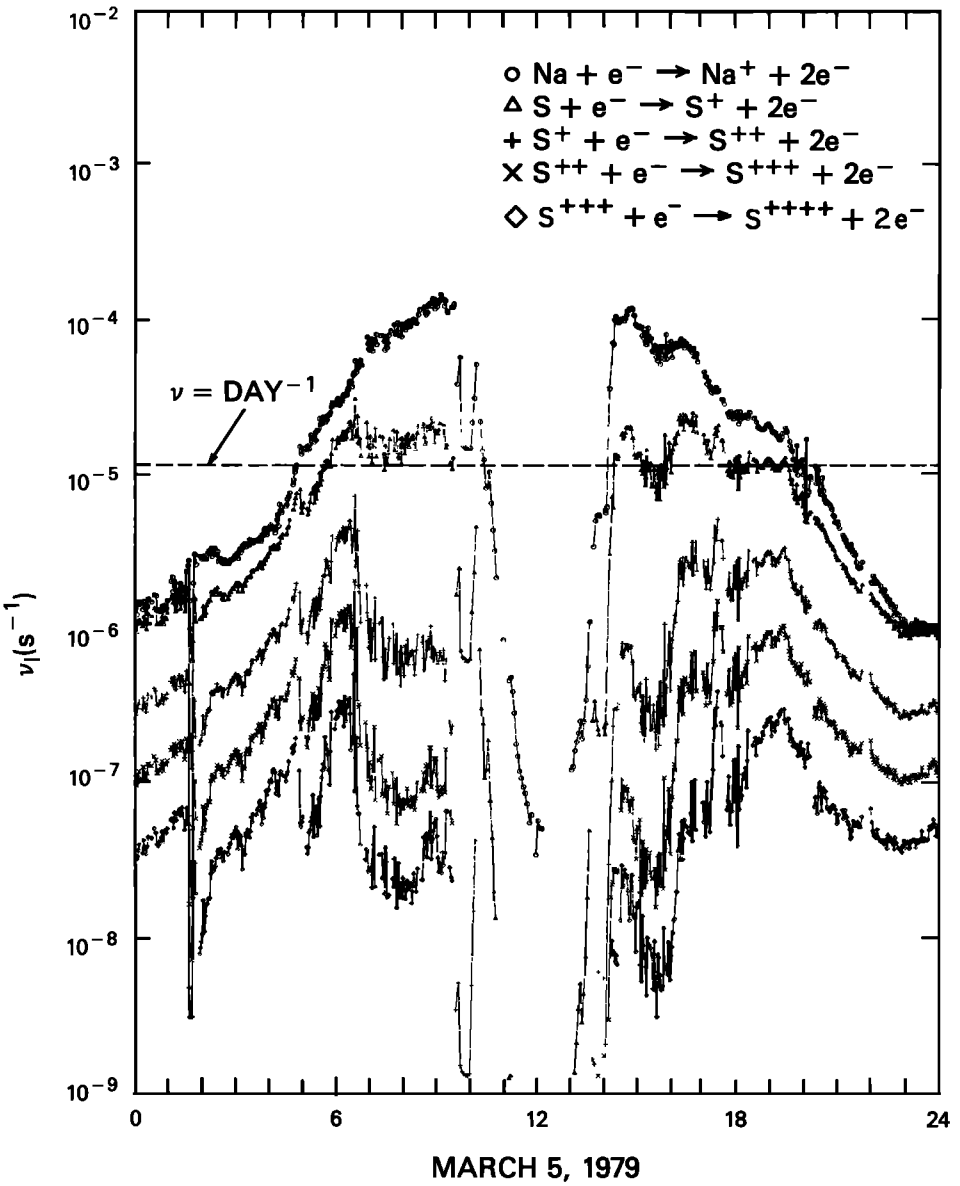

Fig. 11. Plot of electron impact ionization rates along the Voyager 1 trajectory for all of March 5, 1979, for Na (circles), S (triangles), S^+ (pluses), S^{2+} (crosses), and S^{3+} (diamonds).

densities inferred by the Voyager PRA experiment reveals no difference when corrected for latitude. However, the accuracy of PRA densities or model calculations is no better than ~10–20%, so the absence of a change in electron density is not fatal to the dense corona hypothesis.

The Voyager UVS upper limit is 50 R for emission from the vicinity of Io at wavelengths between 1250 and 1450 Å [*Shemansky*, 1980]. Based on the revised *Stone and Zipf* [1974] cross sections for e + O production of 1304-Å photons [*Zipf and Erdman*, 1985], the yield of 1304-Å photons relative to ionization of O is 0.7 at $T_e = 5$ eV. This revised cross section contains a significant contribution due to cascade from higher ^3p terms. Excitation by $T_e = 5$ eV electrons will occur predominantly near threshold for the $^3S^o$ upper term of 1304 Å, and direct excitation should be more important than the cascade contribution. Recent experimental work by *Vaughan and Doering* [1986] indicates 0.6 of the revised Stone and Zipf cross section is due to direct excitation and the net 1304-Å yield relative to ionization approaches 0.4 at $T_e = 5$ eV. In the optically thin limit the 1304-Å intensity produced by electron impact above the exobase would be ~250 R with an assumed yield of 0.4. With the substantial reduction in the electron impact cross section for 1304-Å photons, the electron impact excitation rate and intensity for semiforbidden O I 1356-Å radiation should be comparable to that of 1304 Å at $T_e \sim 5$ eV.

Because the O column density above the exobase is 3×10^{14} cm^{-2}, the optical thickness at line center for 1304 Å is $\tau \sim 28$. In addition, resonance scattering of solar 1304-Å photons by this oxygen corona would produce an additional ~8 R of 1304-Å radiation. Radiative transfer at moderate optical depth introduces two important, opposing effects. Self-absorption tends to reduce the emergent intensity, whereas multiple scattering increases the emergent intensity.

The total estimated intensity of 1304-Å emission from the oxygen corona is estimated at 260 R, which when averaged over the Voyager UVS slit for the range given by *Shemansky* [1980] reduces to 35 R, i.e., below his upper limit. With the

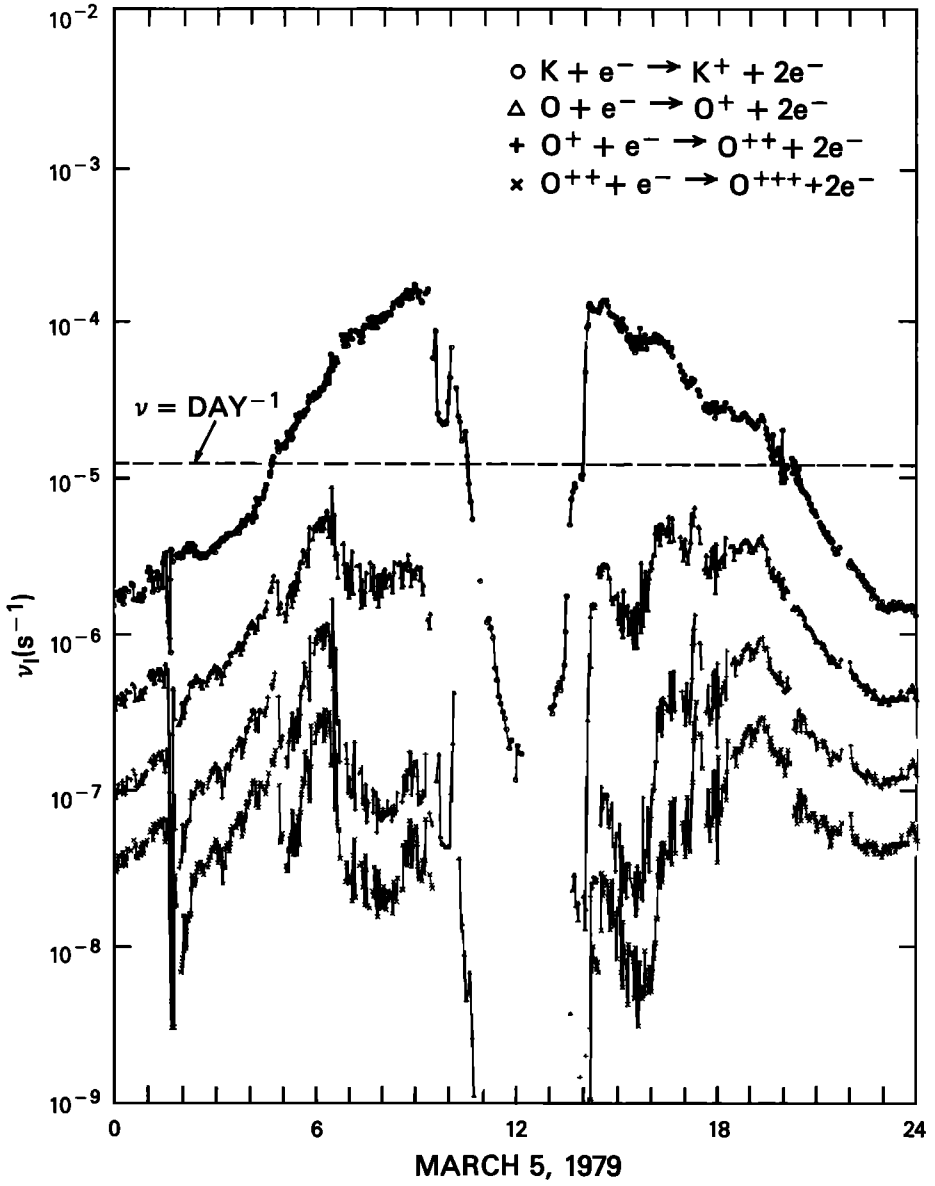

Fig. 12. Plot of electron impact ionization rates along the Voyager 1 trajectory for all of March 5, 1979, for K (circles), O (triangles), O^+ (pluses), and O^{2+} (crosses).

exobase at 2 R_{Io} the corresponding ionization rate of atomic oxygen is $\sim 7 \times 10^{26}$ ions s^{-1}. For neutral sulfur a density approximately an order of magnitude less than the oxygen density is consistent with inferences from (7) and the theoretical models of Summers et al. (1987). Electron impact on sulfur would produce ~110 R of 1429-Å radiation based on *Ho and Henry*'s [1985] collisions strength and $\sim 4 \times 10^{26}$ S^+ ions s^{-1}. Averaged over the UVS slit, the 110 R is equivalent to 15 R and below the limits of detectability by the UVS. There are strong theoretical reasons for expecting a dense neutral corona around Io (Summers et al., 1987), and it is imperative to detect optical emissions from neutrals around Io or set an upper limit as low as 5 R on 1304- and 1429-Å emissions to make progress in understanding the corona.

In addition to ionization of neutrals in this corona around Io there would be substantial amounts of charge exchange which would lead to the creation of hot ions and energize the torus. With the *Johnson and Strobel* [1982] cross sections and the *Smith and Strobel* [1985] ion composition, the charge exchange rate integrated over a cylindrical corona of diameter 2 R_{Io} corresponds to an energy input to the plasma torus of $\sim 1.4 \times 10^{11}$ W. Electron impact ionization followed by pickup of the ions yields another 6×10^{10} W. Thus ionization and charge exchange processes occurring in this neutral corona would supply ~10% of the new plasma and energy to replenish plasma lost by outward radial diffusion and balance EUV radiative power loss, respectively. Critical velocity ionization may also occur, although there is no universally accepted mechanism to evaluate this possibility.

7. Electron Impact Ionization Rates

One straightforward calculation that can be carried out with the plasma electron data base is the ionization rates of neutrals and ions along the Voyager 1 trajectory. In Figures 11 and 12 the ionization rates of the indicated neutrals and ions are illustrated. These rates are the reciprocal of the ioni-

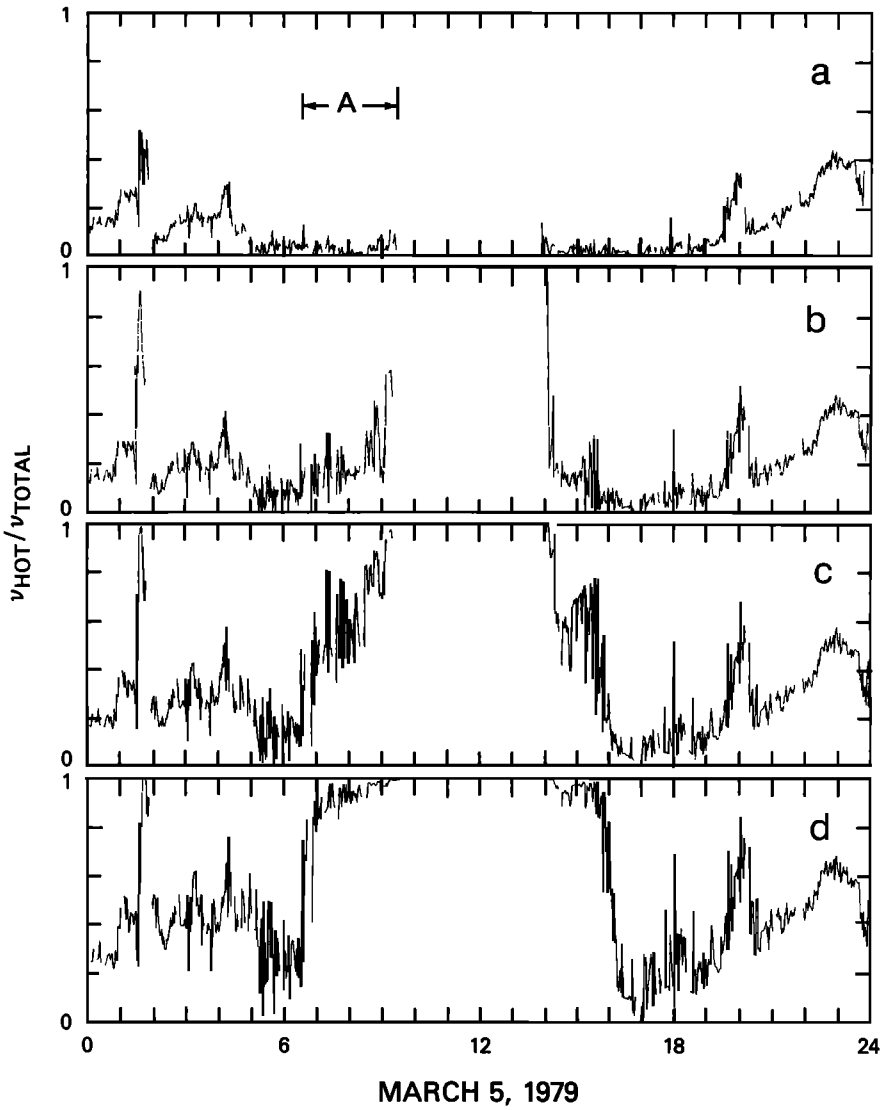

Fig. 13. Plot of fractional ionization rates for the hot electrons ν_{hot}/ν_{total} for all of March 5, 1979, for (*a*) S, (*b*) S^+, (*c*) S^{2+}, and (*d*) S^{3+}. The analysis is preliminary for the time period A when ion feedthrough corrections are important (see text).

zation lifetimes τ_i and were computed with the electron distribution function by the expression

$$\tau_i^{-1} = 4\pi \int_0^\infty \sigma_i(v) f_e(v) v_e^3 \, dv_e$$

where $\sigma_i(v)$ is the ionization cross section. The laboratory cross-section measurements for O by *Brook et al.* [1978] and for O^+ and O^{2+} by *Aitken and Harrison* [1971] were adopted. For sulfur species the laboratory cross-section measurements for S by *Ziegler et al.* [1982] were used; for S^+, S^{2+}, and S^{3+} the semiempirical expressions of *Lotz* [1967] that were used by *Jacobs et al.* [1979] were adopted. Lotz's expressions were also used to calculate Na and K ionization rates, shown in Figures 11 and 12, respectively. For S^{2+}, S^{3+}, O^+, and O^{2+} these calculations are extremely sensitive to threshold cross-section behavior at low electron temperatures. The raw laboratory data were adjusted to ensure that the cross sections smoothly approached zero at threshold to remove any contribution from ionization of excited states.

From Figures 11 and 12, typical lifetimes against ionization can be extracted for the hot torus. Sodium and potassium atoms have a typical lifetime of $\sim 10^4$ s against electron impact ionization along the centrifugal equator and $\sim 2 \times 10^4$ s at higher latitudes, i.e., 1 R_J above and below the equator. In the inner torus their ionization lifetime increases substantially, approaching 10^7 s at 5 R_J. This is, of course, consistent with the observational data base that the extended sodium cloud is inside Io's orbit [cf. *Pilcher and Strobel*, 1982]. The lifetime of neutral sulfur against electron impact ionization in the hot torus is $\sim 5 \times 10^4$ s; whereas for O it is $\sim 5 \times 10^5$ s along the equator. At higher latitudes these lifetimes increase by a factor of 2. In the inner torus these lifetimes increase substantially, exceeding 10^9 s at 5 R_J. As a consequence of these long lifetimes in the inner torus, charge exchange processes control the lifetime of O and S there [*Johnson and Strobel*, 1982]. In the hot torus the lifetime of S^+ against electron impact ionization is $\sim(2\text{–}4) \times 10^6$ s; whereas the lifetimes of S^{2+} and O^+ are $(1\text{–}4) \times 10^7$ s. The greater variation in lifetimes of S^{2+} and O^+ than in lifetimes of O, S, and S^+ in the ramp region $L = 7\text{–}8$ is due to the extreme sensitivity of the lifetime to electron temperature. For example, $T_e \simeq 30$ eV at 0600 and decreases rapidly at $\sim$0630 to a plateau value of 5–6 eV in the hot torus.

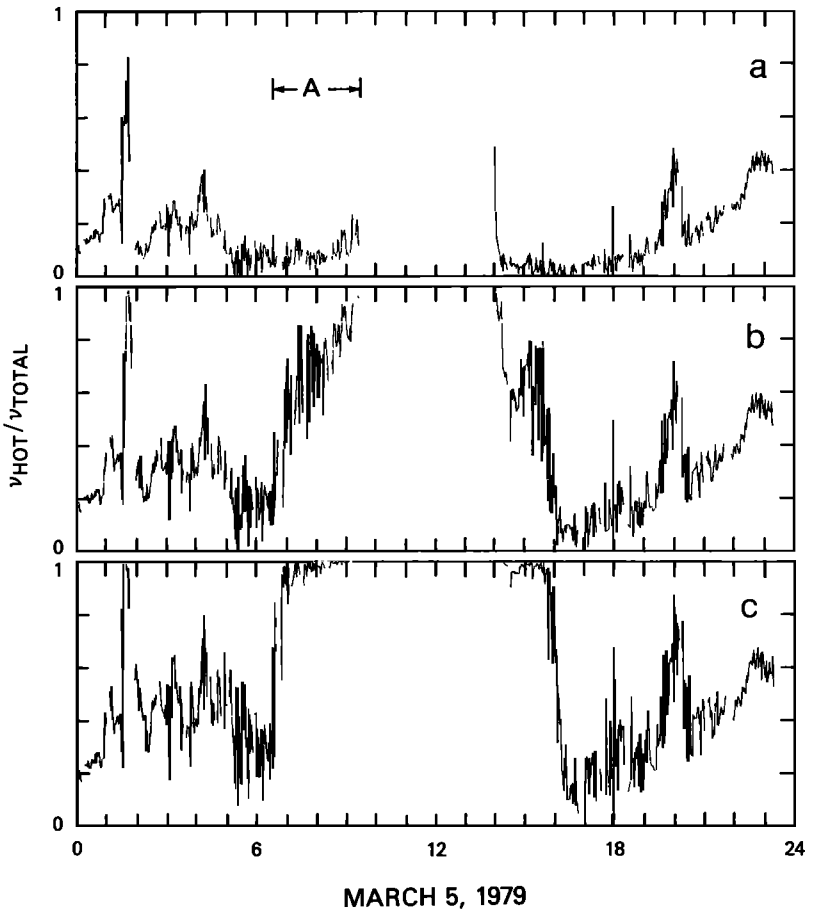

Fig. 14. Same as Figure 13 except fractional ionization rates are for (*a*) O, (*b*) O^+, and (*c*) O^{2+}.

Inside the hot torus the variations in lifetime are due to variations in the density of hot electrons, n_H (cf. Figure 5). This effect is even more evident in the lifetimes of O^{2+} and S^{3+}, which vary from 2×10^7 to 5×10^7 in the hot torus but decrease to $\sim 4 \times 10^6$ s at 0600 and $L = 8$.

The presence of suprathermal electrons with density $n_H \sim 2$ cm^{-3} in the hot torus yields an upper limit of $\tau_i \sim 5 \times 10^7$ s for O^{2+} and S^{3+} and $\sim 1.6 \times 10^7$ s for O^+ and S^{2+}. In regions where τ_i is significantly less than these values, the cold electrons control the ionization rates. This effect can be clearly seen in Figures 13 and 14, where we plot the fractional ionization rate due to suprathermal electrons along the Voyager 1 trajectory. In the hot torus the suprathermal electrons make a negligible contribution to the S ionization rate, contribute 20–40% of the S^+ ionization rate, and contribute 50–80% of the S^{2+} ionization rate. In the case of S^{3+}, essentially all the electron impact ionization is due to suprathermal electrons in the hot torus. Because the ionization potentials (I.P.) of S^{2+} and S^{3+} are 35 and 47.3 eV, respectively, and the ionization rates are proportional to $\exp(-\text{I.P.}/T_e)$, it is obvious why in a plasma with $n_H/n_c \sim 10^{-3}$ and $T_c \simeq 5$ eV the suprathermal electrons play a critical role in the ionization balance for multiple-charged ions.

These ionization rates can be combined with ion density data to derive, in principle, the ion residence or confinement time. If strict collisional ionizational-recombination equilibrium held, a $T_e = 5$–6 eV plasma would have comparable amounts of O^+ and O^{2+} [*Jacobs et al.*, 1978], and $\sim 80\%$ of the sulfur would be S^{2+} with 15% S^{3+} and $\sim 5\%$ S^+ [*Jacobs et al.*, 1979]. The inclusions of suprathermal electrons will shift the ionization balance toward more highly stripped ions [*Shemansky*, 1980]. Direct determination of ion concentrations from in situ PLS measurements is complicated by the inability to uniquely infer $n(S^{2+})$ and $n(O^+)$, which have the same charge to mass ratio, and by the hot ion temperatures which smear out individual ion signatures. Remote UV sensing of the Io torus also has a number of problems which prevent a unique interpretation of ion concentrations [*Brown et al.*, 1983*a*; *Smith and Strobel*, 1985]. Thus *Smith and Strobel* [1985] have argued from a theoretical model for the ion distribution functions and observational data that the plasma ion concentrations appropriate to Voyager 1 conditions were $n(S^+) < 350$, $n(S^{2+}) \simeq 430$, $n(S^{3+}) \simeq 10$–25, $n(O^+) \simeq 660$, and $n(O^{2+}) \sim 40$–80 cm^{-3}. These relative ion density ratios can be understood in terms of a finite residence or confinement time for the ions which shifts the ionization balance to less highly ionized species [*Shemansky*, 1980]. *Shemansky* [1980] on this basis inferred a residence time of 100 days when $T_e = 7$ eV. *Smith and Strobel* [1985] preferred a shorter residence time of ~ 60 days and calculated $T_e = 4.8$ eV. The latter inference of residence time was also based on the shape of the ion distribution functions. Because of the uncertainty in ion composition we did not repeat these calculations which would imply a residence time of 60–100 days. It is important to note that this range of residence time implies that the major loss of O^{2+} and S^{3+} in the hot torus is outward radial diffusion, not electron impact ionization. As a consequence, higher ionization stages of O and S (e.g., O^{3+} and S^{4+}) would not be abundant

in the hot torus and to date have not been spectroscopically detected.

Outside the ramp region $L = 7$–7.5, however, the ionization lifetimes of O^{2+} and S^{3+} are comparable to the residence time, and we might expect the formation of detectable amounts of O^{3+} and S^{4+}. In a preliminary analysis of EUV emission from the ramp region, Shemansky and Strobel (unpublished results) found some evidence for S^{4+} and/or O^{3+}. The analysis of PLS data in the middle magnetosphere by *McNutt et al.* [1981], however, did not indicate the presence of significant amounts of O^{3+} at the mass to charge ratio of $5\frac{1}{3}$. One would expect the ionization state of the plasma to be frozen in once it had passed through the ramp region outside of which the ionization rates drop rapidly and outward radial transport is more rapid. The lack of O^{3+} in the Voyager PLS data in the outer magnetosphere may suggest more rapid passage of the plasma through the ramp region than one would infer from the *Siscoe et al.* [1981] and *Smith and Strobel* [1985] results.

The rapid rise in T_e in the ramp region ($L = 7.5$–8) is consistent with the corresponding plunge in electron density if radiative emission in the EUV is a dominant energy loss mechanism. The radiative cooling rate is given by

$$R \propto \frac{n_i n_e}{T_e} e^{-h\nu/T_e}$$

To compensate for a density decrease, the electron temperature must increase. The radiative cooling rate is maximum for fixed plasma density when $T_e \simeq 2h\nu$. With an average value of $h\nu = 15$–18 eV, $T_e = 30$–36 eV results in maximum radiative cooling. This is precisely the observed value of T_e in the $L = 7.5$–8 region. The factor of 10 decrease in n_e through the ramp region lowers the radiative cooling rate by a factor of 100. But the increase in T_e from 5.5 to 30 eV enhances the cooling rate by a factor of 7 for a net factor of 14 decrease in the cooling rate. This reduced rate of cooling is consistent with substantial radiative losses as the plasma radially diffuses outward by centrifugal interchange instability.

8. SUMMARY

We have presented a comprehensive analysis of the Voyager 1 PLS electron observations on March 5, 1979. As first shown by *Scudder et al.* [1981], the plasma electrons within the Io torus and Jupiter's magnetosphere are composed of a thermal (cold) Maxwellian component and a suprathermal (hot) non-Maxwellian component with significant positive radial gradients in T_e. T_e is less than 1 eV in the cold torus ($L < 5.5$), increases to 5–6 eV in the hot torus ($5.5 \leq L \leq 7.6$), and rises abruptly to $T_e \simeq 30$ eV just outside the hot torus ($L > 7.6$) with an asymptotic value of ~ 100 eV at $r > 12\ R_J$. The mean temperature of the hot electrons is $T_H \sim 500$ eV. Within the hot torus the electron temperature T_e is a factor of 10 less than the temperature T_{ion} of the thermal ions.

In the cold torus the PLS instrument detected no suprathermal electron fluxes, which implies $n_H/n_c < 10^{-4}$. In the hot torus, $n_H/n_c \sim (5$–$10) \times 10^{-4}$ was observed, and outside the hot torus, beyond $L = 7.6$, n_H/n_c can exceed 10^{-1}. This latter increase is due primarily to a decrease in n_c. Satellite sweeping of the hot electron fluxes by Europa at $9.4\ R_J$ was observed. This process defines the outer boundary of the hot electron torus, and Coulomb collisions between the cold and hot electrons (sink mechanism) within the cold torus provide the inner boundary ($L = 5.5$). These observations support the theoretical expectations by *Barbosa et al.* [1985], who proposed a localized source for the hot electrons in the hot plasma torus.

An attempt was made to look for any inbound-outbound asymmetry in the cold electron temperature T_c. If one considers the minimum in T_c centered on the Io flux tube passage as a local effect, then T_c outbound tends to be greater than T_c inbound. This difference in temperature tends to become greater as the latitude difference between inbound and outbound trajectories increases. Although this asymmetry could have been caused by a local time [*Sandel and Broadfoot*, 1982; *Shemansky and Sandel*, 1982] or system III [*Dessler and Vasyliunas*, 1979; *Hill et al.*, 1981, 1983] variation, the more plausible interpretation is a latitudinal variation. This asymmetry, if not due to a latitudinal variation, is at variance with prediction 1 by *Dessler and Vasyliunas* [1979] but is qualitatively supportive of the *Hill et al.* [1981] model predictions (see also *Cheng et al.* [1984]).

The inferred outbound latitudinal variation in the hot electron pressure P_H was modeled in terms of the magnetic mirror force and a parallel electric field $E_\parallel$. If we set an upper limit of $E_\parallel \sim 1\ \mu$V/m for the ambipolar electric field based on the centrifugal confinement of the cold ions, then pressure anisotropies $T_\perp/T_\parallel \sim 10$ for the hot electrons were required to produce the more than factor of 5 observed decrease in P_H from $\lambda_M = 0°$ to $\lambda_M = -12°$. Theoretically, such large pressure anisotropies are not expected because of Coulomb collisions and wave-particle interactions driven by such a large pressure anisotropy. Furthermore, from a roll maneuver near the outbound Europa L shell crossing ($r \simeq 9.4\ R_J$), $T_\perp/T_\parallel \sim 1.17$ was estimated for the hot electrons, although chorus emissions outside the hot torus require $T_\perp/T_\parallel \sim 2$. Therefore if we impose the constraint $(T_\perp/T_\parallel)_{EQ} < 2$, then $E_\parallel > 2.5\ \mu$V/m follows. Consideration of the generalized Ohm's law equation shows that unacceptable charge separations would occur in the thermal plasma from such a large $E_\parallel$ and the only way such large $E_\parallel$ can be supported by the plasma is that there be adequate wave turbulence in the plasma to scatter the thermal electrons (Coulomb collisions unimportant) to prevent significant ion-electron drift.

Observed ratios of T_c/T_H were compared with the predictions by *Birmingham et al.* [1981] with regard to the position in frequency of electrostatic half-harmonic emissions relative to the UHR emission line within the torus. For scale lengths of $\sim 1\ R_J$ the time-averaged estimate of T_c/T_H was in good agreement with their predictions; within the hot torus, $T_c/T_H \lesssim 0.02$ for half-harmonic emission above f_{UHR}, and at $L \sim 8$, $T_c/T_H \sim 0.04$ for emission below f_{UHR}. Lack of half-harmonic emission in the cold torus can be attributed to the lower suprathermal electron fluxes in that region (T. J. Birmingham, private communication, 1983). We argued that the lack of chorus emission from 0505 to 0542 reported by *Coroniti et al.* [1984] using Voyager 1 PWS data was caused by a reduction in the suprathermal electron flux. This flux decrease maximized in energy at about 500 eV, which is typical of the resonance energies discussed by Coroniti et al. for chorus emission.

During the Io flux tube passage there was a remarkably symmetric decrease in T_c centered on closest approach to Io. We attributed this localized cooling of electrons to thermal conduction along magnetic flux tubes to a dense neutral corona surrounding Io. At closest approach the flux tubes

sampled by the PLS experiment were draped around Io near Io's exobase. Observations by IUE and Galileo should be able to confirm the presence of this neutral corona which has been predicted theoretically by *Kumar* [1980], *Summers* [1985], and Summers et al. (1987). Recent IUE observations by *Ballester et al.* [1986] have confirmed our prediction for a neutral corona around Io. This neutral corona provides a modest source of energy to the torus ($\sim 2 \times 10^{11}$ W or about 10% of the total EUV emission) due to the production of pickup ions from charge exchange reactions and electron impact ionization.

Finally, in section 7 we presented electron impact ionization rates along the spacecraft trajectory for all of March 5, 1979. Typical lifetimes against electron impact ionization within the hot torus are $\sim 10^4$ s for Na and K; 5×10^4 s for S; 5×10^5 s for O; (2–4) $\times 10^6$ s for S^+; (1–4) $\times 10^7$ s for S^{2+} and O^+; and (2–5) $\times 10^7$ s for O^{2+} and S^{3+}. In the cold torus, lifetimes approach 10^7 s for Na and K, which is consistent with the observational data base that the sodium cloud resides inside Io's orbit [cf. *Pilcher and Strobel*, 1982]. The lifetimes for S and O exceed 10^9 s, which means their lifetimes are dominated by charge exchange reactions [*Johnson and Strobel*, 1982]. Approximately 50% of the ionization for S^{2+} and O^+ and almost all the ionization of S^{3+} and O^{2+} in the hot torus is due to suprathermals. The rise in electron temperature from 5 eV within the hot torus to 30 eV in the ramp region is consistent with radiative emission in the EUV being the dominant energy loss mechanism of the plasma and the tendency for the plasma to maximize its rate of cooling as the electron density drops rapidly below 10^3 cm^{-3} to 10^2 cm^{-3}.

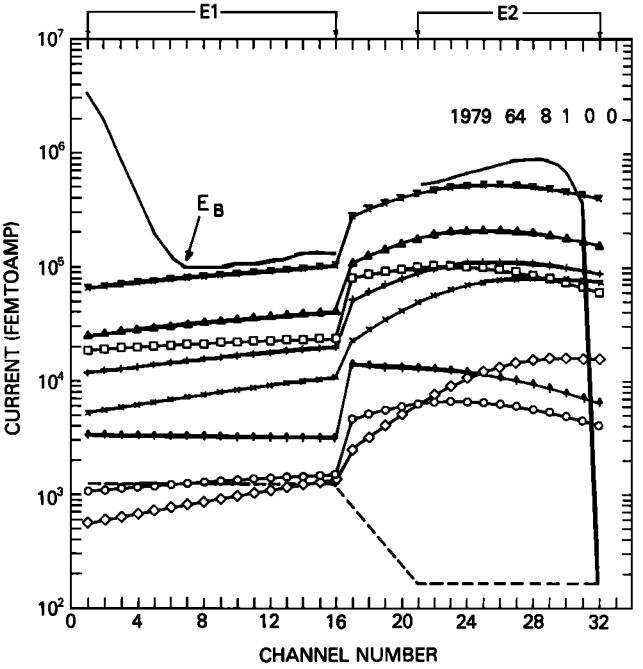

Fig. A1. Plot versus channel number of the observed electron current I_{obs} (solid curve) and ion feedthrough current $(I_{fed}{}^+)_i$ for the different cold ions. Spectrum time is given in upper right-hand corner. The total $I_{fed}{}^+$ is indicated by the crosses with overbars. The symbols used for the other ions are as follows: O^{2+} (open squares), S^{3+} (open circles), S^{2+} (solid triangles), O^+ (pluses), S^+ (crosses), $SO_2{}^+$ (open diamonds), and H^+ (arrows). The ion parameters come from the analysis by *Bagenal and Sullivan* [1981] and *Bagenal et al.* [1985]. The zero telemetry count level is indicated by the dashed line.

APPENDIX

Ion Feedthrough Corrections

As discussed by *Sittler* [1983] (also see *Vasyliunas* [1971]), positive ions entering the D cup when in the electron mode with energies comparable to the current energy level of the instrument will produce an in-phase contaminating signal $I_{fed}{}^+ > 0$. This signal could incorrectly be interpreted as a suprathermal electron component. *Sittler* [1983] also showed that ion impact upon the sensor's modulator grid, with subsequent secondary electron emission, can produce an out-of-phase feedthrough current $I_{fed}{}^- < 0$. This effect becomes important enough for the high-energy electron channels (above a few keV) such that $|I_{fed}{}^-| > |I_{fed}{}^+|$ can occur for the highest-energy channel ($E = 5.2$ keV). The feedthrough current $I_{fed}{}^+$ is caused by the refraction of ion trajectories as they pass through regions of nonzero electric field produced by the modulator grid. Some of these trajectories will be moved on or off the sensor's collector plate as the modulator voltage, with dc level V_M, is varied at 400 Hz with square wave amplitude ΔV_M ($\Delta V_M / V_M \ll 1$). The amplifier and phase detection electronics of the instrument are capacitively coupled to the collector such that only the ac component of the incident current is measured. $I_{fed}{}^-$ is caused by the change in ion energy before it strikes the modular grid as the modulator voltage is varied, coupled with the energy dependence in the secondary electron yield due to ion impact. The net result of these two effects is that they will enhance the suprathermal fluxes below a few keV and cause a possible deficit in fluxes at higher energies, i.e.,

$$I_{obs} = I_e + I_{fed}{}^+ + I_{fed}{}^- \qquad \text{(A1)}$$

with I_{obs} the observed electron current and I_e the incident electron current produced by the ambient plasma electrons.

A third correction not shown in (A1), referred to as I_{sec}, is current produced by electron impact upon the collector with subsequent secondary electron emission which is not successfully returned to the collector by the suppressor grid. This effect can reduce the incident electron current I_e (i.e., $I_{sec} < 0$) by $\lesssim 30\%$ for electron energies $E > 100$ eV and by $\lesssim 10\%$ for $E < 100$ eV.

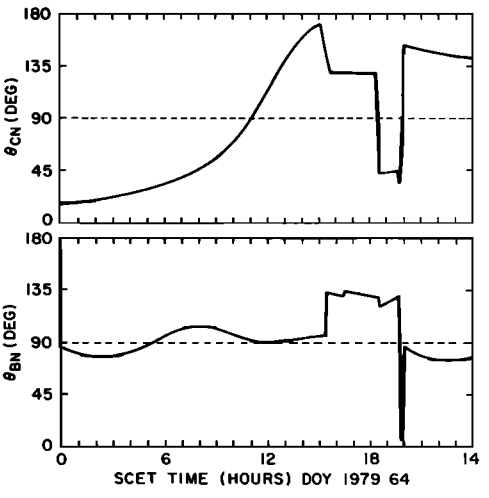

Fig. A2. Plot of the angles θ_{BN} and θ_{CN} versus time for March 5, 1979: θ_{CN} is the angle between the D cup normal $-\hat{n}_D$ and corotation direction, while θ_{BN} is the angle between the magnetic field **B** and $\hat{n}_D$.

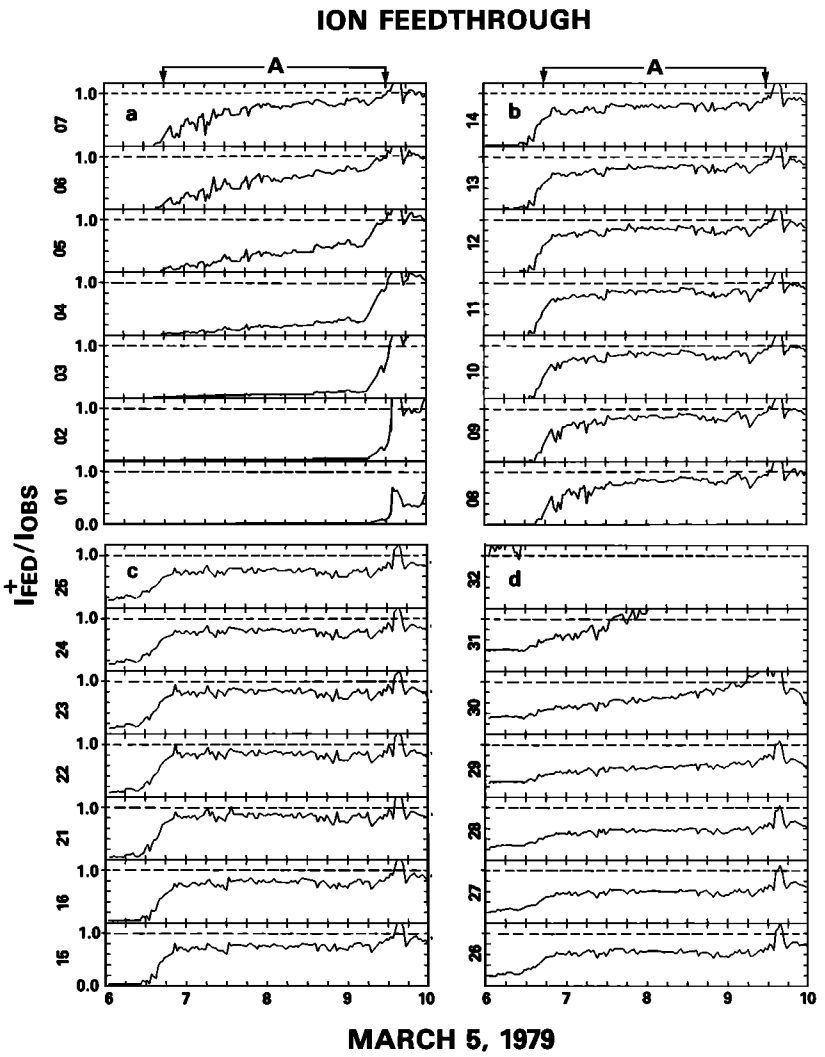

Fig. A3. Plot of $I_{fed}{}^+/I_{obs}$ versus time for all the usable electron speed channels (E1: 1–16 and E2: 21–32). Time period covered is from 0600 to 1000 SCET.

In Figure A1 we have a plot of the observed electron current (solid curve), the total ion feedthrough current $I_{fed}{}^+$ (crosses with overbars), and the ion feedthrough current $(I_{fed}{}^+)_i$ produced by the different ions used in the simulations; the ion parameters come from the analysis by *Bagenal and Sullivan* [1981] and *Bagenal et al.* [1985]. The simulations were performed by a program originally written by V. M. Vasyliunas and later improved by other members of the plasma team. In Figure A2 we plot θ_{BN} and θ_{CN} versus time, where θ_{BN} is the angle between the sensor normal $\hat{n}$ and the ambient magnetic field **B**, and θ_{CN} is the angle between the corotation direction and sensor normal $\hat{n}$ ($\hat{n}$ defined to point into the side sensor). The angle θ_{CN} is 0° for ions flowing directly into the sensor. During the inbound pass the flow is into the D cup, and it becomes more oblique as the spacecraft moves inward, while during the outbound pass the flow is from the back of the sensor except for a roll maneuver between 1820 and 2000 SCET. For the spectrum shown in Figure A1 the ion flow is into the D cup with angle $\theta_{CN} = 45°$, and ion feedthrough corrections are expected to be important.

As can be seen in Figure A1, the cold electrons are totally unaffected by $I_{fed}{}^+$, but the hot electron component above the breakpoint energy E_B is severely affected by $I_{fed}{}^+$, which can be more than 80% of I_{obs}. Except for the upper E2 channels, I_{obs} is greater than $I_{fed}{}^+$ as expected. The sharp turnover in the energy spectrum above 3 keV is probably caused by the dominating influence of $I_{fed}{}^-$. Throughout the inbound passage of the plasma torus when $|I_{fed}{}^+| \sim I_e$ we see this turnover in the spectrum, while during the outbound pass when $|I_{fed}{}^+| \ll I_e$ this effect is generally not seen. It is important to note that $I_{fed}{}^+$ tends to peak at higher energies for those ions of greater mass per charge and thus greater corotational energy per charge. For example, the corotational energy of O^+ at this time is about 364 eV, while for $SO_2{}^+$ it is about 1.45 keV; $I_{fed}{}^+$ due to O^+ peaks at 900 eV, while for $SO_2{}^+$ it peaks at 3.9 keV. Thus for this orientation of the side sensor relative to the corotation direction, $I_{fed}{}^+$ peaks at about 3 times the corotational energy. In these simulations we have not included the contributions provided by the hot ions which can be shown to be generally less than a 10% effect. During the outbound pass at $|\lambda_M| \sim 10°$, where the suprathermal fluxes are lowest, the hot ions may provide a 30% correction. In these regions, $I_{fed}{}^+$ due to the thermal ions is negligible. Corrections due to I_{sec} will tend to offset those produced by the hot ions.

In Figure A3 we display the ratio of $I_{fed}{}^+/I_{obs}$ versus time

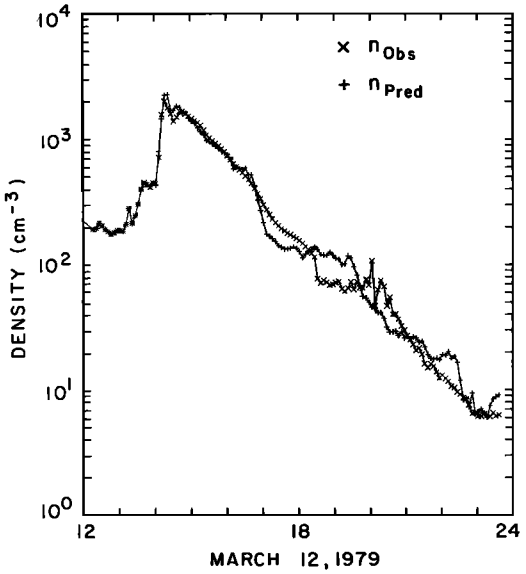

Fig. A4. Time plot of the observed electron density (crosses) and predicted electron density (pluses) from 1200 to 2400 SCET on March 5, 1979 (outbound pass). The predicted estimates were computed from the inbound ion and electron analysis and the dipole part of the O_4 model from *Acuña et al.* [1983].

from 0600 to 1000 SCET. As in Figure A1 we have used the simulation program and ion analysis results from Bagenal and Sullivan and Bagenal et al. The total ion charge densities from *McNutt et al.* [1981], which are weighted sums of the cold and hot ion currents, tend to exceed the total charge densities from Bagenal and Sullivan by 10% ± 5%. We have normalized the total charge densities of Bagenal and Sullivan to equal those of McNutt et al., as a patch to our feedthrough calculations which omit contributions due to the hot ions. When the hot ion parameters become available, the simulations and electron analysis will be repeated to obtain improved suprathermal electron parameters. We have also added a 5% contribution due to H^+ which is shown in Figure A1 to provide a negligible effect. However, within the cold torus, where the flow is more oblique (see Figure A2) and where the ion Mach numbers are larger, the lighter ions such as H^+, which will have a lower Mach number for the same temperature, may provide an important contribution to $I_{fed}{}^+$ at the lower electron energies.

Comparing Figures 3, A2, and A3, one can see the feedthrough corrections do not begin to be important until after 0645, when the densities exceed a few hundred per cubic centimeter and the ion flow is not too oblique in relation to the D cup normal. As expected, the lower channels dominated by cold electron fluxes are almost totally unaffected by $I_{fed}{}^+$. We also see that the upper two E2 channels (31 and 32) are dominated by $I_{fed}{}^+$, which is much greater than the observed current. We think that this is caused by $I_{fed}{}^-$ being large enough so that $I_{obs} < 0$. After 0930 the spacecraft is entering the cold torus, and the suprathermal fluxes are dropping rapidly. At this time the flow is very oblique, and the Mach numbers large enough so that proper modeling of the high-energy tails of the cold ion distributions is required for an accurate estimation of $I_{fed}{}^+$. Also, hot ions probably make a more important contribution to $I_{fed}{}^+$ in this region. For these reasons and the appearance of interference after 1008 we have omitted the inbound analysis after 0933. Simulations based on "predicted" estimates of the ion parameters during the outbound roll maneuver from 1820 to 2000 SCET show that $I_{fed}{}^+$ is less than 10% of I_{obs} for $E < 300$ eV and less than 50% for $E > 300$ eV. Furthermore, during the roll maneuver outbound there is no evidence of a turnover in the E/Q spectrum above a few keV (upper two E2 channels) which indicates that $|I_{fed}{}^-| \ll I_e$.

Spacecraft Charging and Outbound Predicted Densities

In section 3 it was shown that the Voyager 1 spacecraft became negatively charged within the high-density regions of the Io plasma torus where n_e exceeded 1000 cm^{-3}. During the inbound pass when $T_c \approx 5$ eV the spacecraft potential $\Phi_{SC} \approx -10$ V, while during the outbound pass in the outer regions of the torus, $\Phi_{SC} \approx -20$ V when $T_c > 10$ eV. To a first approximation,

$$\Phi_{SC} = -\frac{kT_c}{e} \ln\left(\frac{n_e}{n_e{}^*}\right) \tag{A2}$$

where k is Boltzmann's constant, e is the unit electric charge, $n_e{}^*$ is the electron density estimated from the electron data with $\Phi_{SC} = 0$ V, and n_e is the actual electron density determined from independent estimates (i.e., PRA, PLS ions, etc.). Equation (A2) shows that $|\Phi_{SC}| \propto T_c$ and that $\Phi_{SC} < 0$ for $n_e > n_e{}^*$.

In section 4 we noted that the spacecraft was probably negatively charged between 1830 and 1940 and "predicted" ion charge densities determined from the inbound pass were instead used for n_e. Figure A4 is a plot of the observed electron density n_{obs} (crosses) and predicted electron density n_{pred} (pluses) from 1200 to 2400 on day 64. The observed density n_{obs} is a composite of different data sets as described in section 4 for Figure 3. The predicted density computation is also described in section 4. Between 1636 and about 1900 the spacecraft was in the shadow of Jupiter, and the spacecraft is expected to be negatively charged. From Figure A4 one can see that $n_{pred} \approx n_{obs}$ within the high-density ($n_e > 500$ cm^{-3}) regions of the torus from 1400 to 1700. It can also be seen that azimuthal symmetry is roughly obeyed out to 13 R_J. After about 1830, PRA estimates of n_e were not available, and n_{obs} was computed from the electron data using the return current relation in the work by *Scudder et al.* [1981] (i.e., $\Phi_{SC} > 0$ V assumed). An abrupt decrease in n_{obs} results, which indicates

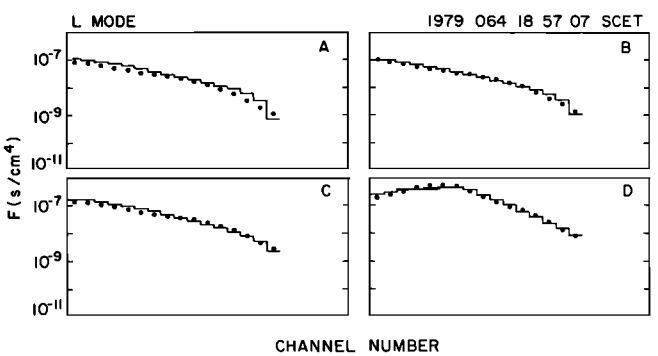

Fig. A5. Fit to the reduced ion distribution function F_i observed by the PLS instrument during the outbound roll maneuver near Europa's L shell when the D cup was aligned to see the nearly corotating cold ions. The data are indicated by the histogram plot while the fit is denoted by the solid circles. See text for details.

that Φ_{SC} is still negative after 1830 and consistent with the spacecraft in Jupiter's shadow until ~1900. Figure A2 shows that a roll maneuver occurs during the time period from 1830 to 1940 when predicted estimates are used. In Figure A5 we show an ion spectrum at 1857 SCET when θ_{CN} was 45°. Superimposed upon the spectrum is a fit to the spectrum which is a modified version of the predicted ion values computed from the inbound analysis of Bagenal and Sullivan. The fit required the addition of hot ion components for O^+, O^{2+}, and S^+ to account for the fluxes in the A, B, and C sensors and a 33% reduction in the cold ion densities relative to their predicted values in order to properly account for the main ion peak in the D cup. When this was done, n_{obs} and n_{pred} were almost identical. It should be noted that the inbound analysis by Bagenal and Sullivan was renormalized to equal the ion charge densities by *McNutt et al.* [1981] which include the contributions of the hot ions to n_e. Though not obvious, one can show that for ion Mach numbers greater than 1 and normally incident flow the estimated ion charge densities using the technique by McNutt et al. are almost exact for both the main and side sensors. Therefore, by renormalizing the analysis by Bagenal and Sullivan we have partially accounted for the hot ion contributions to n_e that were needed to properly fit the ion spectrum in Figure A5. Because of uncertainty in composition for the hot ions in Figure A5, we conservatively estimate that the predicted estimates should be accurate within 30%, if not better. Therefore we conclude that Φ_{SC} is negative for the period that predicted estimates are used and that usage of the predicted estimates for this time interval is warranted.

Acknowledgments. We thank H. S. Bridge for his support and R. L. McNutt, Jr., who graciously provided his preliminary analysis and greatly appreciated technical assistance. We also thank F. Bagenal, who provided the ion parameters which were essential for the successful analysis of the electron data and for pointing out the consequences of a larger $E_{\parallel}$ upon the thermal plasma. J. E. P. Connerney and M. H. Acuña kindly provided information about the MAG team magnetic field model of Jupiter. Useful discussions and assistance from H. K. Wong, A. F. Viñas, M. Desch, J. K. Alexander, T. J. Birmingham, and M. Summers are acknowledged. Comments by A. J. Dessler are also appreciated. D.F.S. was supported by NASA contract NAGW-648 and the Voyager Mission.

The Editor thanks three referees for their assistance in evaluating this paper.

REFERENCES

Acuña, M. H., K. W. Behannon, and J. E. P. Connerney, Jupiter's magnetic field and magnetosphere, in *Physics of the Jovian Magnetosphere*, edited by A. J. Dessler, p. 1, Cambridge University Press, New York, 1983.

Aitken, D. K., and M. F. Harrison, Measurement of the cross-sections for electron impact ionization of multi-electron ions, I, O^+ to O^{2+} to O^{3+}, *J. Phys. B, 4*, 1176, 1971.

Bagenal, F., Variable plasma conditions inside Io's orbit: Voyager measurements, *J. Geophys. Res., 90*, 311, 1985.

Bagenal, F., and J. D. Sullivan, Direct plasma measurements in the Io torus and inner magnetosphere of Jupiter, *J. Geophys. Res., 86*, 8447, 1981.

Bagenal, F., R. L. McNutt, Jr., J. W. Belcher, H. S. Bridge, and J. D. Sullivan, Revised ion temperatures for Voyager plasma measurements in the Io plasma torus, *J. Geophys. Res., 90*, 1755, 1985.

Ballester, G. E., H. W. Moos, D. F. Strobel, M. E. Summers, P. D. Feldman, J. L. Bertaux, M. C. Festou, T. E. Skinner, and J. Lieske, Detection of neutral atomic cloud near Io using IUE, paper presented at Second Neil Brice Memorial Symposium: Magnetospheres of the Outer Planets, Univ. of Iowa, Iowa City, 1986.

Barbosa, D. D., and M. Kivelson, Dawn-dusk electric field asymmetry of the Io plasma torus, *Geophys. Res. Lett., 10*, 210, 1983.

Barbosa, D. D., and W. S. Kurth, Suprathermal electrons and Bernstein waves in Jupiter's inner magnetosphere, *J. Geophys. Res., 85*, 6729, 1980.

Barbosa, D. D., F. V. Coroniti, W. S. Kurth, and F. L. Scarf, Voyager observations of lower hybrid noise in the Io plasma torus and anomalous plasma heating rates, *Astrophys. J., 289*, 392, 1985.

Birmingham, T. J., J. K. Alexander, M. D. Desch, R. F. Hubbard, and B. M. Pedersen, Observations of electron gyroharmonic waves and the structure of the Io torus, *J. Geophys. Res., 86*, 8497, 1981.

Bridge, H. S., J. W. Belcher, R. J. Butler, A. J. Lazarus, A. M. Mavretic, J. D. Sullivan, G. L. Siscoe, and V. M. Vasyliunas, The plasma experiment on the 1977 Voyager mission, *Space Sci. Rev., 21*, 25, 1977.

Broadfoot, A. L., et al., Extreme ultraviolet observations from Voyager 1 encounter with Jupiter, *Science, 204*, 979, 1979.

Brook, E., M. F. A. Harrison, and A. C. H. Smith, Electron ionization of He, C, N, and O atoms, *J. Phys. B, 11*, 3115, 1978.

Brown, R. A., The Jupiter hot plasma torus: Observed electron temperature and energy flows, *Astrophys. J., 244*, 1072, 1981.

Brown, R. A., C. B. Pilcher, and D. F. Strobel, Spectrophotometric studies of the Io torus, in *Physics of the Jovian Magnetosphere*, edited by A. J. Dessler, p. 197, Cambridge University Press, New York, 1983*a*.

Brown, R. A., D. E. Shemansky, and R. E. Johnson, A deficiency of OIII in the Io plasma torus, *Astrophys. J., 264*, 309, 1983*b*.

Carlson, R. W., D. L. Matson, and T. V. Johnson, Electron impact ionization of Io's sodium emission cloud, *Geophys. Res. Lett., 2*, 469, 1975.

Cheng, A. F., M. T. Paonessa, C. G. Maclennan, L. J. Lanzerotti, and T. P. Armstrong, Longitudinal asymmetry in the Io plasma torus, *J. Geophys. Res., 89*, 3005, 1984.

Connerney, J. E. P., M. H. Acuña, and N. F. Ness, Modeling the Jovian current sheet and inner magnetosphere, *J. Geophys. Res., 86*, 8370, 1981.

Coroniti, F. V., F. L. Scarf, C. F. Kennel, W. S. Kurth, and D. A. Gurnett, Detection of Jovian whistler mode chorus: Implications for the Io aurora, *Geophys. Res. Lett., 7*, 45, 1980.

Coroniti, F. V., F. L. Scarf, C. F. Kennel, and W. S. Kurth, Analysis of chorus emissions at Jupiter, *J. Geophys. Res., 89*, 3801, 1984.

Dessler, A. J., Differential rotation of the magnetic fields of gaseous planets, *Geophys. Res. Lett., 12*, 299, 1985.

Dessler, A. J., and V. M. Vasyliunas, The magnetic anomaly model of the Jovian magnetosphere: Predictions for Voyager, *Geophys. Res. Lett., 6*, 37, 1979.

Goertz, C. K., Energization of charged particles in Jupiter's outer magnetosphere, *J. Geophys. Res., 83*, 3145, 1978.

Gurnett, D. A., and F. L. Scarf, Plasma waves in the Jovian magnetosphere, in *Physics of the Jovian Magnetosphere*, edited by A. J. Dessler, p. 285, Cambridge University Press, New York, 1983.

Gurnett, D. A., W. S. Kurth, and F. L. Scarf, Auroral hiss observed near the Io plasma torus, *Nature, 280*, 767, 1979.

Hill, T. W., A. J. Dessler, and L. J. Maher, Corotating magnetospheric convection, *J. Geophys. Res., 86*, 9020, 1981.

Hill, T. W., A. J. Dessler, and C. K. Goertz, Magnetospheric models, in *Physics of the Jovian Magnetosphere*, edited by A. J. Dessler, p. 353, Cambridge University Press, New York, 1983.

Ho, Y. K., and R. J. W. Henry, Oscillator strengths and collision strengths for neutral sulfur, *Astrophys. J., 90*, 424, 1985.

Hultqvist, B., On the interaction between the magnetosphere and the ionosphere, paper presented at the STP Symposium, Leningrad, USSR, May 1970.

Hultqvist, B., On the production of a magnetic-field-aligned electric field by the interaction between the hot magnetospheric plasma and the cold ionosphere, *Planet. Space Sci., 19*, 749, 1971.

Ip, W., and G. Goertz, An interpretation of dawn-dusk asymmetry of UV emission from the Io plasma torus, *Nature, 302*, 232, 1983.

Jacobs, V. L., J. Davis, and J. E. Rogerson, Ionization equilibrium and radiative energy loss rates for C, N, and O ions in low density plasmas, *J. Quant. Spectrosc. Radiat. Transfer, 19*, 591, 1978.

Jacobs, V. L., J. Davis, J. E. Rogerson, and M. Blaba, Dielectronic recombination rates, ionization equilibrium, and radiative energy-loss rates for neon, magnesium, sulfur ions in lower-density plasmas, *Astrophys. J., 230*, 627, 1979.

Johnson, R. E., and D. F. Strobel, Charge exchange in the Io torus and exosphere, *J. Geophys. Res., 87*, 10385, 1982.

Kennel, C. F., and H. E. Petschek, Limit on stably trapped particle fluxes, *J. Geophys. Res.*, *71*, 1, 1966.

Kumar, S., A model of the SO_2 atmosphere and ionosphere of Io, *Geophys. Res. Lett.*, *7*, 9, 1980.

Kurth, W. S., F. L. Scarf, D. A. Gurnett, and D. D. Barbosa, A survey of electrostatic waves in Saturn's magnetosphere, *J. Geophys. Res.*, *88*, 8959, 1983.

Lotz, W., Electron-impact ionization cross-sections and ionization rate coefficients for atoms and ions, *Astrophys. J. Suppl. Ser.*, *14*, 207, 1967.

McNutt, R. L., Jr., J. W. Belcher, and H. S. Bridge, Positive ion observations in the middle magnetosphere of Jupiter, *J. Geophys. Res.*, *86*, 8319, 1981.

Moreno, M. A., and D. D. Barbosa, Mass and energy balance of the cold Io torus, *J. Geophys. Res.*, *91*, 8993, 1986.

Pilcher, C. B., and J. S. Morgan, The distribution of S[II] emission around Jupiter, *Astrophys. J.*, *238*, 375, 1980.

Pilcher, C. B., and D. F. Strobel, Emissions from neutrals and ions in the Jovian magnetosphere, in *Satellites of Jupiter*, edited by D. Morrison, p. 807, University of Arizona Press, Tucson, 1982.

Pilcher, C. B., J. H. Fertel and J. S. Morgan, S[II] images of the Io torus, *Astrophys. J.*, *291*, 377, 1985.

Roesler, F. L., F. Scherb, and R. J. Oliversen, Periodic intensity variations in S[III] 9531 A emission from the Jupiter plasma torus, *Geophys. Res. Lett.*, *11*, 128, 1984.

Sandel, B. R., Corotation lag in the Io plasma torus—Evidence from Voyager EUV observations (abstract), *Bull. Am. Astron. Soc.*, *15*, 810, 1983.

Sandel, B. R., and A. L. Broadfoot, Io's hot plasma torus: A synoptic view from Voyager, *J. Geophys. Res.*, *87*, 212, 1982.

Sandel, B. R., et al., Extreme ultraviolet observations from Voyager 2 encounters with Jupiter, *Science*, *206*, 962, 1979.

Scarf, F. L., D. A. Gurnett, and W. S. Kurth, Jupiter plasma wave observations: An initial Voyager 1 overview, *Science*, *204*, 991, 1979*a*.

Scarf, F. L., F. V. Coroniti, D. A. Gurnett, and W. S. Kurth, Pitch-angle diffusion by whistler-mode waves near the Io plasma torus, *Geophys. Res. Lett.*, *6*, 653, 1979*b*.

Scudder, J. D., E. C. Sittler, Jr., and H. S. Bridge, A survey of the plasma electron environment of Jupiter: A view from Voyager, *J. Geophys. Res.*, *86*, 8157, 1981.

Shemansky, D. E., Mass-loading and diffusion-loss rates of the Io plasma torus, *Astrophys. J.*, *242*, 1266, 1980.

Shemansky, D. E., Ratio of oxygen to sulfur in the Io plasma torus, *J. Geophys. Res.*, *92*, 6141, 1987.

Shemansky, D. E., and B. R. Sandel, The injection of energy into the Io plasma torus, *J. Geophys. Res.*, *87*, 219, 1982.

Shemansky, D. E., and G. R. Smith, The Voyager 1 EUV spectrum of the Io plasma torus, *J. Geophys. Res.*, *86*, 9179, 1981.

Siscoe, G. L., A. Eviatar, R. M. Thorne, J. D. Richardson, F. Bagenal, and J. D. Sullivan, Ring current impoundment of the Io plasma torus, *J. Geophys. Res.*, *86*, 8480, 1981.

Sittler, E. C., Jr., Plasma electron analysis: Voyager plasma science experiment, *NASA Tech. Memo.*, *85037*, 1983.

Sittler, E. C., Jr., K. W. Ogilvie, and J. D. Scudder, Survey of low-energy plasma electrons in Saturn's magnetosphere: Voyager 1 and 2, *J. Geophys. Res.*, *88*, 8847, 1983.

Smith, R. A., and D. F. Strobel, Energy partitioning in the Io plasma torus, *J. Geophys. Res.*, *90*, 9469, 1985.

Stern, D. P., One-dimensional models of quasi-neutral parallel electric fields, *J. Geophys. Res.*, *86*, 5839, 1981.

Stone, E. J., and E. C. Zipf, Electron-impact excitation of the $^3S^o$ and $^5S^o$ states of atomic oxygen, *J. Chem. Phys.*, *60*, 4237, 1974.

Summers, D., and G. L. Siscoe, Calculation of charge-state ratios for satellite tori, *Geophys. Res. Lett.*, *12*, 753, 1985.

Summers, M. E., Theoretical studies of Io's atmosphere, Ph.D. thesis, Calif. Inst. of Technol., Pasadena, 1985.

Thorne, R. M., Jovian auroral secondary electrons and their influence on the Io plasma torus, *Geophys. Res. Lett.*, *8*, 509, 1981.

Trafton, L., Jovian SII torus: Its longitudinal asymmetry, *Icarus*, *42*, 111, 1980.

Trauger, J. T., G. Munch, and F. L. Roesler, A study of the Jovian [SII] nebula at high spectral resolution, *Astrophys. J.*, *236*, 1035, 1980.

Vasyliunas, V. M., Deep-space plasma measurements, in *Methods of Experimental Physics*, vol. 9B, *Plasma Physics*, edited by R. H. Lovberg, p. 49, Academic, Orlando, Fla., 1971.

Vasyliunas, V. M., Plasma distribution and flow, in *Physics of the Jovian Magnetosphere*, edited by A. J. Dessler, p. 395, Cambridge University Press, New York, 1983.

Vaughan, S. O., and J. P. Doering, Absolute experimental differential and integral electron excitation cross sections for atomic oxygen, 2, The ($^3P \rightarrow {}^3S^o$) transition (1304 Å) from 16.5 to 200 eV with comparison to atomic hydrogen, *J. Geophys. Res.*, *91*, 13,755, 1986.

Warwick, J. W., et al., Voyager 1 planetary radio astronomy observations near Jupiter, *Science*, *204*, 955, 1979.

Winske, D., M. Tanaka, C. S. Wu, and K. B. Quest, Plasma heating at collisionless shocks due to the kinetic cross-field streaming instability, *J. Geophys. Res.*, *90*, 123, 1985.

Ziegler, D. L., J. H. Newman, L. N. Goeller, K. A. Smith, and R. F. Stebbings, Single and multiple ionization of sulfur atoms by electron impact, *Planet. Space Sci.*, *30*, 1269, 1982.

Zipf, E. C., and P. W. Erdman, Electron impact excitation of atomic oxygen: Revised cross sections, *J. Geophys. Res.*, *90*, 11,087, 1985.

E. C. Sittler, Jr., NASA Goddard Space Flight Center, Code 692, Greenbelt, MD 20771.

D. F. Strobel, Department of Earth and Planetary Sciences, Johns Hopkins University, Baltimore, MD 21218.

(Received December 20, 1985;
revised December 23, 1986;
accepted January 15, 1987.)